Report Series in Radiochemistry 23/2004

Inorganic ion exchangers for decontamination of radioactive wastes generated by the nuclear power plants

Risto Koivula

Helsinki 2003

University of Helsinki
Faculty of Science
Department of Chemistry
Laboratory of Radiochemistry
Finland

INORGANIC ION EXCHANGERS FOR DECONTAMINATION OF RADIOACTIVE WASTES GENERATED BY THE NUCLEAR POWER PLANTS

Risto Koivula

Academic Dissertation

To be presented with the permission of the Faculty of Science of the University of Helsinki for public criticism in Auditorium A129 of the Kumpula Chemistry Department on May 28th, 2003, at 12 o'clock noon.

Helsinki 2003

Custos:
Prof. Olof Solin
Laboratory of Radiochemistry
Department of Chemistry
University of Helsinki
Finland

Opponent:
Prof. Markku Leskelä
Laboratory of Inorganic Chemistry
Department of Chemistry
University of Helsinki
Finland

Reviewers:
Prof. Michael Streat
Department of Chemical Engineering
Loughborough University
United Kingdom

Prof. Mark Weller
Laboratory of Structural and Materials Chemistry
Department of Chemistry
University of Southampton
United Kingdom

ISSN 0358-7746
ISBN 952-10-1184-X (nid.)
ISBN 952-10-1185-8 (PDF)
http://ethesis.helsinki.fi
Yliopistopaino
Helsinki 2003

Abstract

Large volumes of radioactive waste have accumulated in the past six decades of nuclear power generation. The forthcoming decommissioning of nuclear power plants will only add to the extremely wide range of nuclear waste solutions already in existence. Decontamination of these wastes before final disposal or release to nature is a demanding task, which requires extremely effective materials and techniques. Ion exchange is considered to be an effective separation technique and, with novel selective ion exchange materials, it has the potential for radioactive waste management.

The focus of this study was materials useful in the separation of activated corrosion products from waste solutions, and in particular a material selective for nickel uptake was sought. In view of the good chemical and physical characteristics in ion exchange processes shown by tin antimonates, an extensive series of tin antimonates was synthesised with 0% to 100% degree of Sn/Sb substitution. The tin antimonates were categorised by structure into pyrochlore (Fd3m, antimony pentoxide), rutile ($P4_2/mnm$, tin dioxide) and a mixture of these metal oxides and this division was clearly reflected in the ion exchange properties of the materials.

The ion exchange properties of the pyrochlore-structured tin antimonates were associated with their tunnel structure, which could be modified by Sn for Sb substitution. Increased Sn content in the pyrochlore lattice improved the metal uptake of the material. Increased Sb content in rutile-structured tin antimonates also improved the metal uptake, but this was attributed to increased electrostatic attraction of the materials. The metal uptake properties of the mixed metal oxides varied widely and were related to the degree of Sn/Sb substitution of the material and to the physical form of the material.

The ion exchange performance of tin antimonates was highly promising for the separation of activated corrosion products. Distribution coefficients for cobalt and nickel were high and developed in parallel fashion as a function of Sn/Sb substitution, although at considerably different levels. In dynamic column experiments, large volumes of solutions up to 25 000 bed volumes, were decontaminated to a high level of purity. In some cases, the physical characteristics of the material resulted in clogging of the column, suggesting the need for further modification before their use in real applications.

Preface

The work presented in this thesis was carried out in the Laboratory of Radiochemistry at the University of Helsinki, during the years 1999-2003.

I wish to express my sincerest gratitude to Professor Timo Jaakkola and to Docent Jukka Lehto for the opportunity to start and carry out studies in the pleasant atmosphere of the Laboratory of Radiochemistry.
I am most grateful to Docent Risto Harjula for taking control of our ion exchange group and for his invaluable support for bringing my postgraduate studies to conclusion. Without the support and input from the ion exchange group: Markku, Kaisa, Teresia, Pasi, Heikki and co-author Airi this study would have never been.
I am also grateful to all my fellow workers for that warm atmosphere and taking part in activities both inside and outside the laboratory. Especially members of the orienteering club RaSu and our talented floorball team are gratefully acknowledged. For keeping me in right direction and giving faith to the future my warmest thanks to Teija.

Co-operation between the different laboratories of the Department of Chemistry has been essential for this study and many persons in the Laboratory of Inorganic Chemistry and in the Laboratory of Polymer Chemistry are warmly thanked.

Dr Kathleen Ahonen and Anthony Meadows are warmly thanked for revising the language of the thesis and the articles.

Financial support from the Academy of Finland, National Technology Agency of Finland, Fortum and Jenny and Antti Wihuri Foundation is gratefully acknowledged.

List of original papers

The thesis is based on the following publications and manuscript, hereafter referred to by their Roman numerals (I–V).

I Koivula, R., Harjula, R. and Lehto, J., Structure and ion exchange properties of tin antimonates with various Sn and Sb contents, *Microporous and Mesoporous Materials*, 2002, 55, 231-238

II Koivula, R., Harjula, R. and Lehto, J., The effect of 0-100% Sn/Sb substitution on nickel uptake of tin antimonates, *J. Mater. Chem*., 2002, 12, 3615-3619

III Koivula, R., Paajanen, A., Harjula, R. and Lehto, J., Decontamination of radioactive cobalt, nickel, strontium and cesium from simulate solutions using tin antimonate columns, submitted to *Solvent Extraction and Ion Exchange*

IV Koivula, R., Harjula, R. and Lehto, J., ^{63}Ni and ^{57}Co uptake and selectivity of tin antimonates of different structure, accepted for publication in *Separation Science and Technology*

V Koivula, R. and Lehto, J., Ion exchange of radionuclides on natural and modified mica minerals, *Radiochemistry*, 1998, 40(6), 507-510

Abbreviations

AAS	atomic absorption spectrometry
AMP	ammonium molybdophosphate
BT	breakthrough
BV	bed volumes
CST	crystalline silicotitanate
DF	decontamination factor
DTA	differential thermal analysis
FDW	floor drain water
HCF	hexacyanoferrate
IEC	ion exchange capacity
IUPAC	international union of pure and applied chemistry
NPP	nuclear power plant
p.z.c.	point of zero charge
PAN	polyacronitrile
Purex	plutonium uranium redox extraction
SBU	secondary building unit
SDVB	polystyrenedivinylbenzene
SIXEP	site ion exchange effluent plant
TG	thermogravimetric
XRD	X-ray diffraction
XRF	X-ray fluorescence
ZrP	zirconium phosphate

CONTENTS

1. Introduction

Use of fission reactors for production of energy generates considerable amounts of radioactive wastes in almost all phases of the nuclear fuel cycle. Removal of the radionuclides of most concern, the long-lived transuranium elements and fission products, from the waste effluents, has been studied and executed by a number of different techniques for the last six decades. Ion exchange, as one of those techniques, has been employed with good results along with other separation techniques (e.g. precipitation and adsorption). Most of the ion exchangers that have been used are organic resins, but also some inorganic exchangers, e.g. natural zeolites and some synthetic materials, have been adopted in nuclear waste treatment. The present strict regulations on discharging toxic metals to the environment have focused interest on inorganic ion exchangers, which generally possess much better selectivity than ordinary organic resins for the radionuclides of concern. High selectivity is one of the key factors in nuclear power plant (NPP) waste management since the radioactive nuclides are present in trace concentrations in complex solutions. Moreover, these solutions contain high concentrations of inactive ions that interfere with the uptake of radionuclides. Also the physical characteristics, good resistance to decomposition at elevated temperatures and at high fields of ionising radiation, have been regarded as an advantage for inorganic ion exchangers in nuclear waste management.

A number of nuclear reactors have already been shut down, and most of the operating NPP are approaching their licensed operating time and their decommissioning is becoming relevant. The decontamination of these materials produces large amounts of radioactive solutions that have to be treated before their storage or release to the environment.

This dissertation focuses on inorganic ion exchange materials that could be used to obtain high separation of radionuclides from waste effluents and decrease their release to the environment. After a brief history of inorganic ion exchangers, modern ion exchange materials are introduced, both ones in use and ones that have the potential to be used in radioactive waste treatment. The theory of ion exchange is presented to the extent needed to understand the concepts of ion exchange used in this study. The main part of the dissertation concerns tin antimonates: their synthesis, structure and ion exchange properties. These are discussed in detail. In addition, the results of a study of

the uptake of radionuclides on mica minerals are included bringing some perspective in evaluating the performance of the synthetic materials.

1.1 Background

The history of ion exchangers is remarkably long. One of the oldest applications of inorganic ion exchangers was the purification of seawater with a layer of sand, something that was known to Aristotle in the fourth century BC. The first scientific experiments with inorganic ion exchangers were done with zeolite chabazite, as reported in the mid-19th century by Thompson, Way and Eichhorn.[1] Coincidentally, clinoptilolite, a material isomorphous to chabazite, is presently in use for Cs and Sr separation at Sellafield nuclear fuel reprocessing plant.[2-3] The weak chemical stability of the early inorganic ion exchangers led to the development and synthesis of organic ion exchangers (organic resins) in the 1930s. With few exceptions, organic resins, based on a chemically very stable polystyrenedivinylbenzene (SDVB) backbone, replaced the inorganic ion exchangers.

The needs of the nuclear industry – high selectivity, tolerance for ionising radiation and possibly high temperatures – were the basis for the further development of inorganic ion exchangers. Since the mid 1960s, after the appropriate analytical techniques and knowledge of ion exchange processes became available, new inorganic materials were synthesised and studied with particular attention to the relation of structure to the ion exchange properties of the material.[4-5] Hundreds of inorganic materials have been synthesised, studied and tested for use in radioactive waste treatment. Also, materials with better chemical stability than zeolites were and are still being sought amongst natural minerals.

1.2 Ion exchangers in use in the nuclear power industry

At the moment, organic resins are used in almost every step of the nuclear fuel cycle. Ion exchange resins are used at NPPs (depending on the reactor type) for purification and chemical control of primary coolant water, polishing of steam condensate, production of make-up water, purification of spent fuel storage pond water and treatment of waste solution. In the case of waste solution, one of their functions is to

remove radioactive ionic contaminants, mainly caesium, and radioactive particulate contaminants, such as cobalt and nickel, in order to prevent radiation build up in the reactor system.[6] Typically two different kinds of ion exchange process are employed: conventional deep bed columns and precoat filters. In these processes the ion exchange resins function as ion exchangers for the ionic contaminants and as mechanical filters for particulate contaminants. Ion exchange resins are of strong acidic (sulfonic $–SO_3^-$) or strong basic (quaternary $–N(CH_3)_3^+$) type, of macroporous structure for the column bed and of gel type for precoat filter applications.[7] Depending on the reactor, separation of ionic contaminants has been 90-100% and separation of particulate contaminants 40-95%. The ion exchangers used in NPPs are almost without exception of nuclear grade, which means normal organic resins of high quality, low in metallic impurities and coherent in particle size. Annual consumption of organic resins in an operating reactor may be as high as 10 tonnes, and for the final disposal the resins will be incinerated or mixed directly with cement.

For their part, inorganic ion exchangers in NPPs have primarily been used in the decontamination of radioactive waste solutions originating from drain waters, decontamination operations and leaks of different kinds. A common approach to dealing with these wastes has been concentration by evaporators, but solidification by precipitation or ion exchange has also been applied before final disposal. Dozens of different materials and combinations of materials have been tested with varied success, but only a few groups of materials have shown constant and good performance in radionuclide separation.[8-13] The use of inorganic exchangers has decreased the volume of the concerned wastes considerably and generated substantial economic savings.[14-15]

At the moment several different inorganic ion exchangers are used in NPPs and fuel reprocessing plants and some of them even in large-scale applications. Among these materials the natural zeolite clinoptilolite is used for caesium separation in large scale at the SIXEP process in the Sellafield fuel reprocessing plant. In addition, hexacyanoferrates such as CsTreat®, which are far more selective for caesium than zeolites, are used at several sites instead of evaporator concentration.

1.3 Modern inorganic ion exchangers for separation of radionuclides

The needs of the nuclear industry have been the catalyst for the development of modern inorganic ion exchangers. The number of inorganic ion exchange materials is great and their classification somewhat difficult. Ion exchangers have been classified in terms of their structure and ion exchange properties but also in terms of their origin. Here a rough classification of inorganic ion exchangers into naturally occurring and synthetic materials is applied. These two groups are then divided into smaller subgroups that better reflect the physical and chemical properties of the materials.

1.3.1 Natural inorganic ion exchangers

Almost all natural minerals act as ion exchangers. In general, clay minerals, zeolites and oxides, particularly silicon oxides, are categorised as natural inorganic ion exchangers, even though in many cases they are synthetic. When they are used in naturally occurring form, it is mainly because of their low production costs, but in some cases also because of their unique chemical and physical characteristics.

Clay minerals are phyllosilicates at advanced weathered stage with a particle size < 4 μm and a two-dimensional or layered structure. The 2:1 and 1:1 layered structure is built up of silicon oxide tetrahedra and octahedra with magnesium as the central cation (figure 1a). Isomorphous substitution of Al^{3+} for Mg^{2+} and Al^{3+} for Si^{4+}, which generates an excess negative charge on the structure, leads to an uncountable number of clay minerals. Clay minerals are primarily cation exchangers, though they possess anion exchange properties as well, to a much lesser extent. The two-dimensional layer structure of clay minerals is more or less rigid, and most of the anisometric ion exchange sites lie on the surfaces of the material. This means that the surfaces may exhibit several kinds of dissociable groups resulting from the isomorphous substitution. The layer structure allows the expansion of some clay minerals, but it also gives the material no or only a small ion sieve effect, which somewhat decreases its selectivity. Clays have been studied mainly for agricultural applications such as fertilisers, and much ion exchange data have been published in that connection. Clay minerals have been used as a barrier against radionuclide pollution in uranium mining areas and the clay mineral bentonite will serve this use in final nuclear waste repositories.

Mica minerals are phyllosilicates too. Although closely associated with the clay mineral group, with their unique three-layer structure (figure 1b) they are more properly treated as a group of their own. The three-layer structure of mica minerals is constructed from two tetrahedral layers with an octahedral layer in between. Tetrahedra are built from silicon oxide, where silicon is the central cation and three oxygen atoms are shared with adjacent tetrahedra. All tetrahedra are oriented in such a manner that, between two tetrahedral layers, an octahedral layer is formed from the remaining oxygen atoms of the tetrahedra. Usually the central cation in the octahedra is divalent iron or magnesium of coordination number six. Two hydroxyl groups are shared between three neighbouring octahedra. The central cation in both of the tetrahedral and the octahedral layers can be replaced by a trivalent cation such as iron or aluminium.[16] When iron replaces silicon in the tetrahedral layer, a negative charge is generated in the structure. In the case that iron replaces magnesium in the octahedral layer, a positive charge is created. The net charge of a three-layer unit is thus negative, and the negative charge is balanced by an interlayer cation that binds the three-layer units together. The two main categories of micas based on their layer charge density are (a) true micas with one negative charge per formula unit and (b) brittle micas with two negative charges per formula unit.[16] The interlayer cations, which are exchangeable, make the structure of mica minerals more or less expandable. In addition, silicon hydroxide groups are present at the crystal edges of mica minerals and make a slight contribution to the ion exchange properties of the mineral.[17]

Differences in the structure and ion exchange properties of mica minerals have been studied, for example, by changing the interlayer cations and replacing the centre ions of tetrahedra and octahedra. As well, the synthesis of new micas with charge densities of 2, 3 and even 4, using cheap starting materials like kaolin and magnesium oxide, have been studied with the aim of producing commercially competitive, highly selective ion exchangers.[18-23]

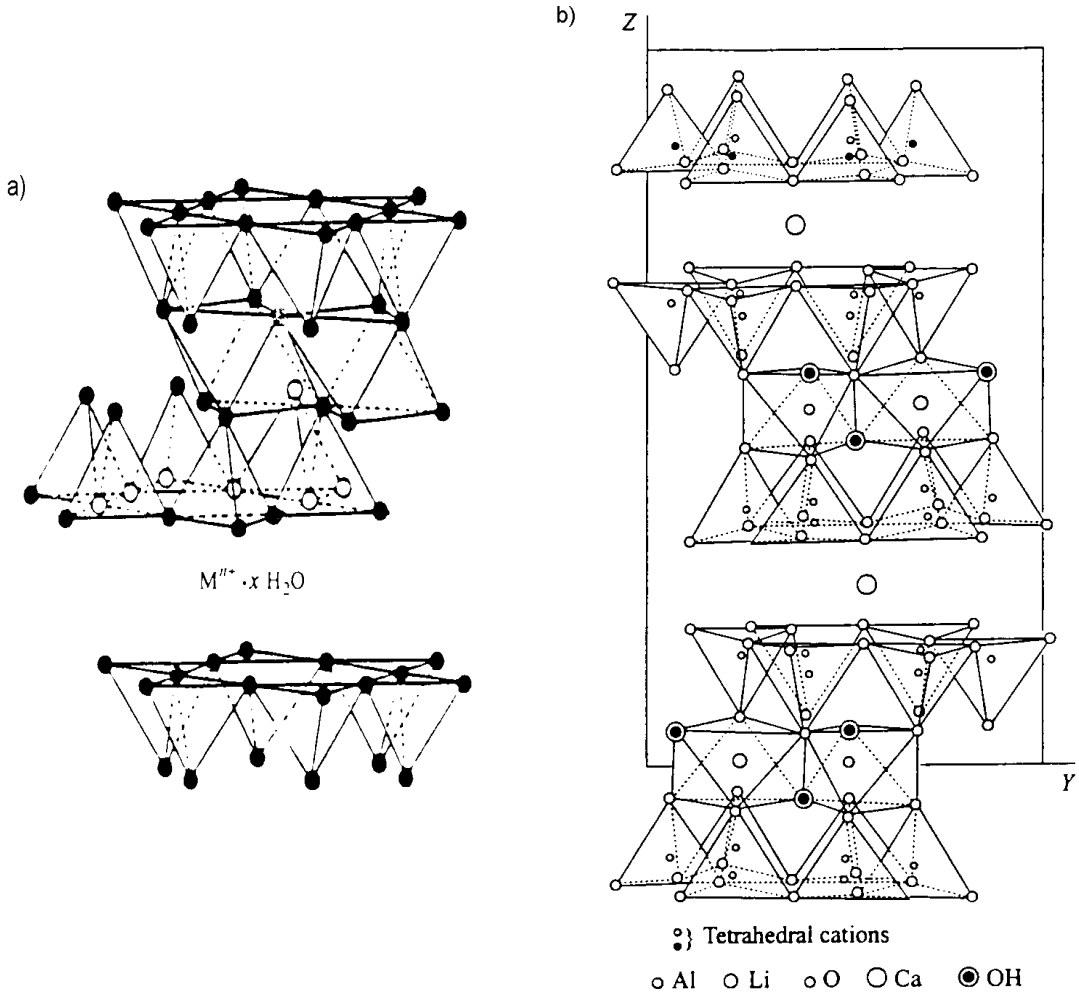

Figure 1. Structures of (a) layered (2:1) clay mineral, and (b) brittle mica mineral (margarite-$2M_1$).

Zeolites are crystalline hydrated aluminosilicates ($M_{2/n}OAl_2O_3 \bullet xSiO_2 \bullet yH_2O$, where M is a nonframework cation with valence n and $x \geq 2$). Their structure is built up of tetrahedral SiO_4 and AlO_4 units bridged by oxygen atoms generating secondary building units (SBU). The SBUs may be connected in several different ways resulting rigid, three-dimensional structures with tunnels and cavities (pore size typically from 4 to 10 Å) where the exchangeable ions are located. The trivalent aluminium in the structure generates a negative charge in the framework that imparts the ion exchange properties to the material, i.e. one mole of Al produces one equivalent of cation exchange capacity in the framework. The typical ion exchange capacity of high Al content zeolites is close to 5 meq/g and as a result of their three-dimensional structure they have good selectivity for certain elements (ion sieve effect). The ion exchange properties of zeolites have been studied extensively[24-26] but their great variety in structure and ion exchange

properties precludes a detailed presentation of ion exchange data here. Although the ion exchange properties of zeolites are good, their operating pH range is relatively narrow due to the dissolution of Si in alkaline and Al in acidic solutions. This has somewhat hindered their use.[27] Over 100 different zeolites are known today and new materials with structures close to zeolites are continually being synthesised. In addition, a vast amount of zeolites are synthesised for the detergent industry, where zeolites are used as water softeners.

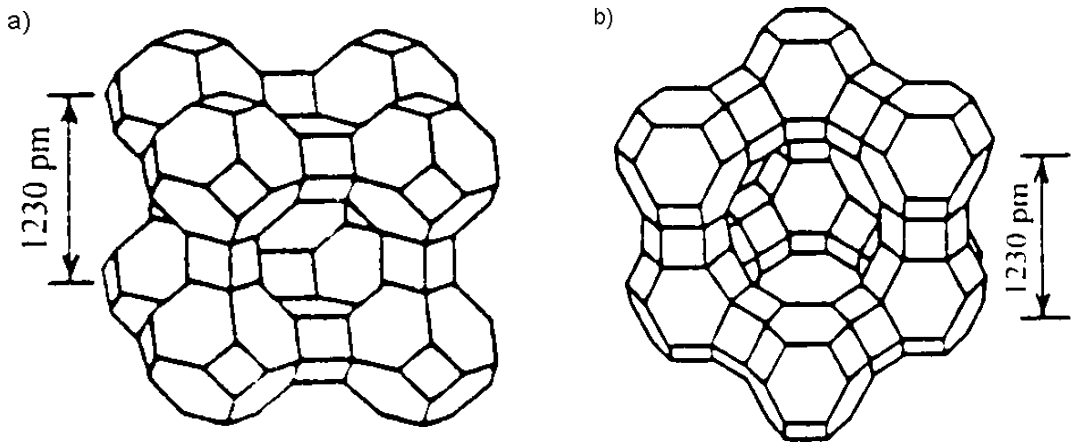

Figure 2. Schematic representation of framework of (a) zeolite A (synthetic), and (b) faujasite (natural) zeolites.

1.3.2 Synthetic inorganic ion exchangers

Since the first industrially synthesised inorganic ion exchangers (aluminosilicate gels in 1905)[1], higher selectivity and better tolerance for harsh condition have been the goals for every material scientist synthesising new inorganic ion exchangers. Synthetic inorganic ion exchangers can be divided into several categories, such as acid salts, insoluble ferrocyanides, hydrous oxides, salts of heteropoly acids and other ionic compounds. Some of the materials fall into several of the categories on the basis of their physical and chemical properties, which somewhat confuses the division. The following materials have already been demonstrated or are considered as promising inorganic ion exchangers for radionuclide separations.

Acid salts are a large group of ion exchangers, amongst which tetravalent cations Zr, Th, Ti, Sn are most studied, followed by some trivalent cations such as Al and Cr. The anions most extensively employed include phosphate, arsenate, antimonate, vanadate

and molybdate. Acid salts have gel or microcrystalline structure and their composition and properties are easily modified by the conditions of synthesis. Their composition is most likely non-stoichiometric and the proportion of cations, anion groups and water vary widely affecting the ion exchange properties of the material. The hydrogen atoms bound to the anionic groups create the ion exchange properties, and the selectivity depends on the size of the exchanging cations and cavities and the distances between layers of the material. In particular, the hydration size and energy of the exchanging cations has a great effect on the selectivity of tunnel- and layer-structured materials. If the material has high charge density it can strip or partly strip away the hydration shell of cations, decreasing their size and enabling their access to the inner structure of the material.

The knowledge obtained in ion exchange studies of crystal α-zirconium phosphate ($Zr(HPO_4)_2 \times H_2O$,(ZrP)) has enabled a better understanding of the general mechanisms of the ion exchange process, and ZrP is probably the most studied inorganic ion exchanger (figure 3).[4,28-31] The ZrP exchanger is layered in structure with interlayer distances of 7.6 Å, and 5.3 Å between the nearest P–OH groups. Van der Waals forces between water molecules of the structure and P–OH groups bind the different layers together. Both hydrogen atoms are exchangeable but they are exchanged one at a time, altering the structure as they leave and in turn altering the selectivity sequence of the material. Hydrogen-form ZrP is caesium selective, but the selectivity sequence changes ($Cs^+ > Rb^+ > K^+ > Na^+$) as a function of loading.[32-33] Further making ZrP of interest is the high ion exchange capacity (6.63 meq/g).[34]

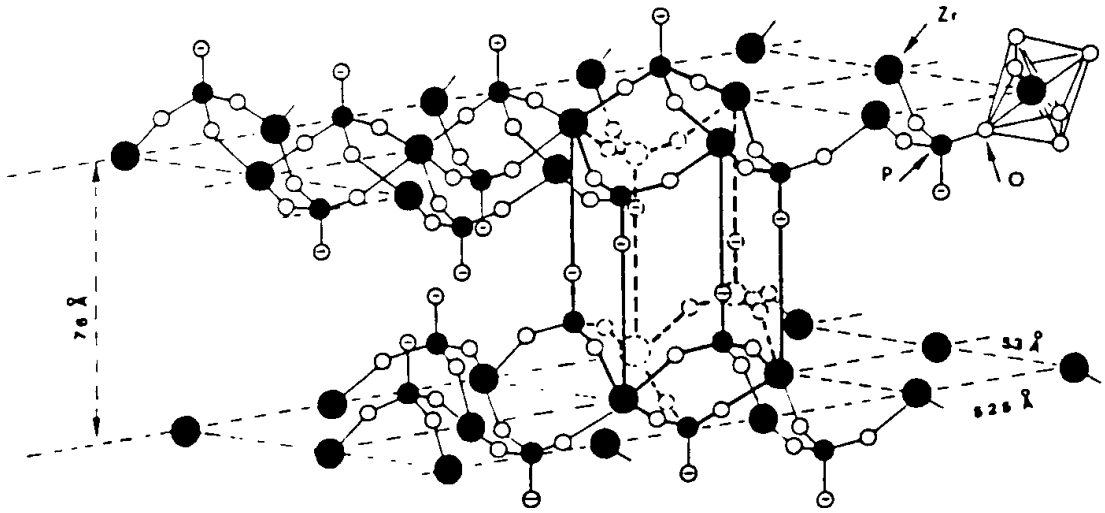

Figure 3. Structure of two-layer α-zirconium phosphate (ZrP).[34]

Hexacyanoferrates (HCF) are superb inorganic materials for the removal of caesium from high concentrations of alkali metals and they have been used for that purpose for decades. HFC complexes may be synthesised in either Fe(II) or Fe(III) form, and mixing them with a solution of a transition metal salt solution usually precipitates a small particle or colloidal product.[35-37] Precipitation with a heavy metal, such as cobalt, eventually results in granulate HCF of high chemical stability and extremely good selectivity for caesium, and such materials have even been used in industrial scale.[38-39] The high caesium selectivity of $K_2[CoFe(CN)_6]_2$, for example, can be attributed to the size of the cavities in the HCF structure, which almost exactly accommodate unhydrated caesium ions.[40] The ion exchange of Co-HCFs occurs on the outermost surfaces of the particle, resulting in relatively small ion exchange capacity (IEC) of ~0.4 meq/g, while the IEC of Zn-HFC may exceed 6.0 meq/g indicating ion exchange on the internal surfaces.[36,41] Peptization of HCFs in neutral and alkaline solutions has been observed, but with some granulated heavy metal HCFs it becomes a limiting factor only above pH 13.

Hydrous oxides are solids with an oxide–water system, where the water molecules are fairly strongly bound to the metal hydroxide groups at the surface of the material. However there is no evidence of definite hydrates, and hydrous oxides of stoichiometric composition are scarce. Hydrous oxides exhibit both cationic and anionic exchange properties depending on the surrounding medium. This amphoteric ion exchange behaviour is attributed to the surface of the material and its point of zero charge (p.z.c.). The p.z.c. is specific for different materials and it determines, together with the pH of the surrounding medium, whether the material acts as a cation or anion exchanger. The exchange reaction of hydrous oxides can be expressed as follows:

$$M\text{—}OH + N^+ \rightleftharpoons M\text{—}ON + H^+ \quad (1)$$

$$M\text{—}OH_2^+ + N^- \rightleftharpoons M\text{—}OH_2N \quad (2)$$

or

$$M\text{—}OH + N^- \rightleftharpoons M\text{—}N + OH^- \quad (3)$$

(M represents the central atom of the ion exchanger phase and N represents the exchanging ion from the initial solution).

In basic solution the reaction of equation 1 is dominant and the material behaves as a cation exchanger, whereas in acidic solution equation 2 (or 3) is valid and the material behaves as an anion exchanger. In addition, the acidity of hydrous oxides is often used

in almost the same way as the p.z.c., that is, to determine what kind of ion exchange properties the material has. The acid strength of a compound increases with the addition of oxygen ($MO<M_2O_3<MO_2<M_2O_5<MO_3$), resulting in cation exchange properties at low pH values. In addition, the polarisation of the anion (oxygen of the OH group) increases with the cation ionic potential (φ)[42], which is defined by the relation

$$\varphi = \text{cation charge} / \text{cation radius} \qquad (4)$$

The higher the ionic potential (φ) the more acidic the material, and the better the cation exchange properties at low pH values.

Hydrous oxides may be divided into two main types: framework hydrates and particle hydrates.[34] Framework hydrates are generally formed by pentavalent elements from groups 5 and 15 and they typically have poorly crystalline structure. The crystallinity can usually be enhanced by hydrothermal treatment or by refluxing the material in acidic medium, but this may change the selectivity of the material.

One of the best studied framework hydrates is antimony pentoxide (Sb_2O_5), which is known for its excellent uptake of strontium.[42] Pyrochlore-structured Sb_2O_5 has a tunnel structure, which allows cations of diameter smaller than 6 Å (in two directions) to penetrate to the inner ion exchange sites of the material.[42-43] The size of the tunnels is too small for most of the hydrated metal ions, so that partial dehydration of the ions must occur before ion exchange. Owing to this ion sieve effect of the framework hydrates, their selectivity is a compromise between hydration and electrostatic forces.

Particle hydrates, mostly formed by elements from groups 3, 4, 13 and 14, are characterised by having a bulk structure that resembles one of their ceramic oxides. Their surface is largely covered with hydroxyl groups, which are easily affected by a change in pH of the surrounding medium, and changes in the ion exchange properties result. In addition, owing to the low orientation and small crystal size characteristic of particle hydrates, the ion sieve effect of the structure is rather small. An example of particle hydrates is rutile tin dioxide (SnO_2), which is one of the materials of interest in this study, and is described in detail later in the text.

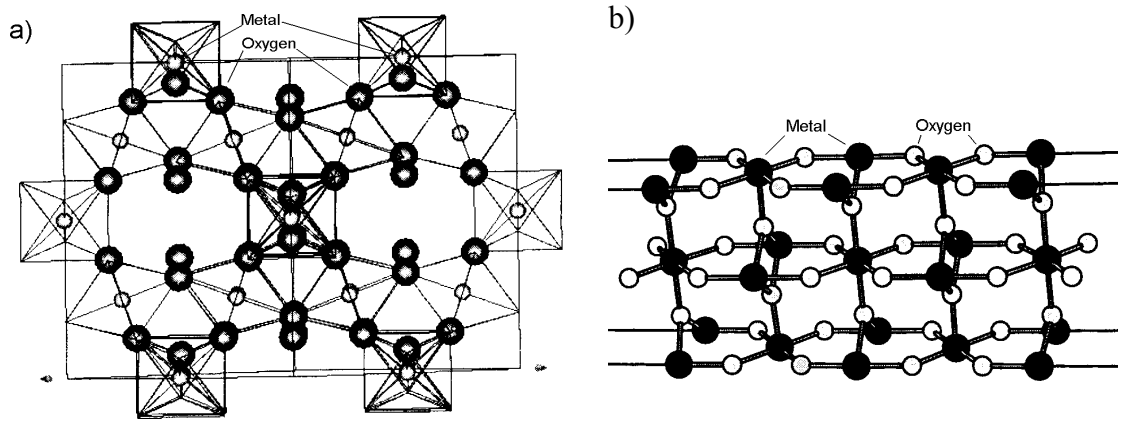

Figure 4. Structures of a) pyrochlore and b) rutile materials.

Interesting ion exchange properties have been observed for hydrous mixed metal oxides. Sodium titanates (ideal formula $Na_4Ti_9O_{20}\bullet nH_2O$) have been found particularly selective for strontium in alkaline solutions of high sodium content. The layer structure of sodium titanate is built up of chains of three edge-sharing TiO_6 octahedra, connected through their corners to the next unit of three octahedra, and thus giving rise to layers. The exchanging sodium ions are located between the layers. The interlayer distance has a great effect on the ion exchange properties of crystalline-layered materials and the distance for hydrous-form sodium titanate is 9.7 Å (typically 3 to 15 Å in titanates). This is large enough for most of the hydrated metal cations, and high ion exchange capacities, up to 9 meq/g, have been measured for titanates. Owing to the weakly acidic character of the material, their performance in acidic conditions is poor.

The **salts of heteropoly acids** are a much smaller group of ion exchangers than the groups discussed above. A good example of their structure is provided by ammonium molybdophosphate ($(NH_4)_3PMo_{12}O_{40}$, AMP), where phosphorus is surrounded tetrahedrally by four groups of three MoO_6 octahedra (figure 5).[44] The octahedra are bridged by one or two oxygen atoms and the ammonium and water molecules are located between the $[P(Mo_3O_{10})_4]^{3-}$ complexes. The exchange of ammonium is followed by rearrangement of the remaining ammonium ions to form a stronger hydrogen bond array and restructuring of the heteropoly anion. This change in structure does not favour further exchange, and the exchange process is incomplete. Molybdenum phosphates are perhaps the most interesting heteropoly acids, of which ammonium molybdophosphate (AMP) is the most thoroughly studied.[45-47] AMP has mainly been tested for caesium separation, but also chromatographic separation of mono-, di- and trivalent cations can be achieved with proper variation of the eluent.[48] Diffusion within the structure of

heteropoly acids is rather slow, but their particle size is also very small (generally they are powders) so that equilibrium is achieved within reasonable time. Owing to the small particle size of AMP, its use in column applications has not been entirely successful and has encouraged further development of the material. Granulate composite material of AMP with polyacrylonitrile (PAN) support has shown potential for caesium uptake in column experiments. Also other support materials have been tested.[49-51]

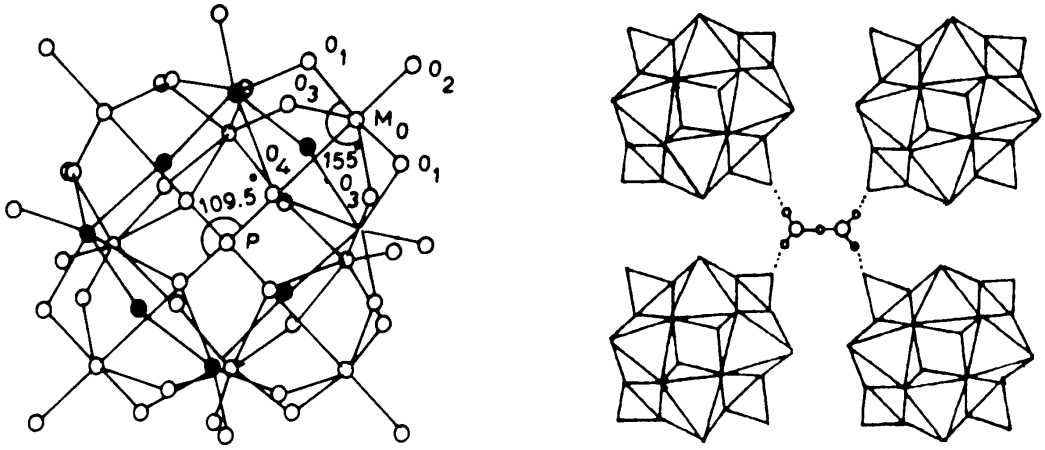

Figure 5. The 12-molybdophosphate anionic unit and its secondary structure.[47,52]

Most naturally occurring inorganic ion exchangers are based on silicon oxides, but also many synthetic ion exchange materials exploit the tetrahedral structure of silicon tetroxides. One promising silicon-based framework compound is a titanium **silicate** ($Na_2Ti_2O_3(SiO_4)\times 2\ H_2O$, crystalline silicotitanate (CST)), which is highly selective for Cs and somewhat also for Sr in NaOH and sodium-bearing solutions.[53] The framework of CST is formed of four corner-sharing TiO_6 octahedra bridged by SiO_4 tetrahedra in the a- and b-axes (figure 6). Bridging oxo-groups connect the octachedra resulting in a tetragonal unit cell (a = b = 7.8Å, c ≅ 12Å) and tunnelled structure. Sodium ions are located between the octahedral layers connecting the silica tetrahedra.[54] The tunnel size is suitable for caesium ions and CST is one of the most promising materials for caesium separation.[55-57] At high alkalinities, the interference of sodium with caesium uptake is significant, but selectivity for caesium can be enhanced by substitution of Nb^{5+} ions for Ti^{4+}. This will reduce the ion exchange capacity of the material, however. The size of the tunnels also limits the use, as ions larger than sodium are not fully exchanged. For example, only ~60% of the ion exchange capacity of CST is utilised in potassium exchange.[34]

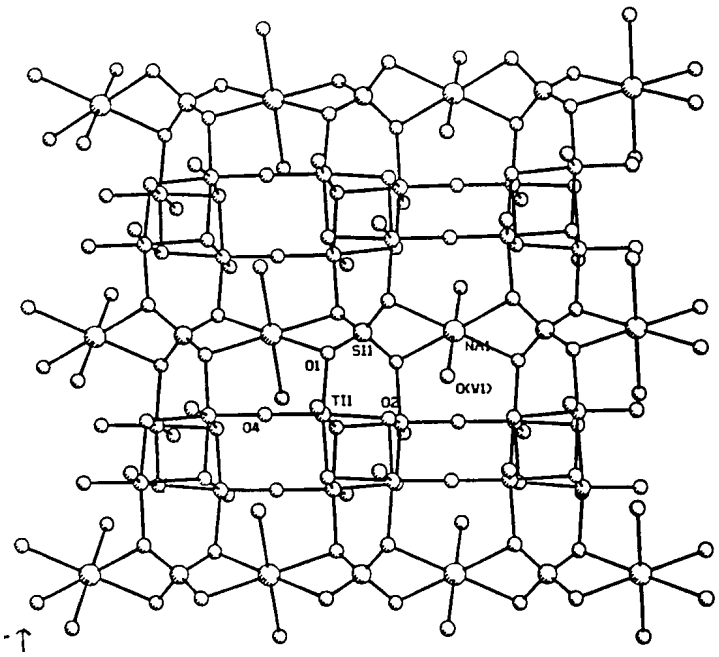

Figure 6. Structure of $Na_2Ti_2O_3(SiO_4)\times 2\ H_2O$ (CST).[54]

Closely related to the titanosilicates are a group of materials with structure resembling that of the mineral pharmacosiderite ($HM_3Ti_4O_4(SiO_4)_3\bullet 4H_2O$ where M is univalent ion).[34] A difference between the two groups of materials is that the latter have a cubic structure with unit cell a = 7.821 Å in both hydrogen and caesium forms.[58] The cubic structure has a clear influence on the ion exchange behaviour, though both types of material have good caesium and strontium ion exchange properties.[59]

Pyrochlore-structured antimony silicates (SbSi) are highly selective for strontium in acidic solutions, which is a rare property for inorganic ion exchange materials. Apparently the silicon replaces antimony in site A in the pyrochlore structure ($A_2B_2O_6O'$), which somewhat decreases the ion exchange capacity of the material (2.7 meq/g for Na^+ compared with 5.1 meq/g for Na^+ in the case of hydrous antimony pentoxide).[60] This lower affinity for sodium has a positive effect on strontium selectivity in sodium-bearing solutions. The affinity of antimony silicates for caesium is relatively modest but it can be improved by doping with Nb^{5+} and W^{6+} ions. The strong interference by sodium ions remains however.[61-62]

Many inorganic solids are ionic and exhibit ion exchange properties (broadly speaking) and these are usually referred to as **other ionic compounds** in the ion exchange literature. This group is extensive, including all manner of insoluble materials (halides, sulphides, carbonates and perchlorates). As an example of these, sulphates have been used for the separation of radioactive strontium and radium.

1.4 Radionuclides of interest

Corrosion and wear occur in the primary circuit of the cooling system of a nuclear reactor. **Activated corrosion products** of NPP are produced by neutron activation of a corrosion product deposit on the fuel surface or by activation of in-core structure materials inside the reactor. The main corrosion products and their activated radionuclides are presented in Table 1. The activated corrosion products are released from the fuel surface by dissolution and erosion caused by coolant flow. In addition, dissolution and wear releases activated nuclides, mainly ^{58}Co and ^{60}Co, from the in-core structure.

Table 1. Main corrosion products and their activation schemes; half-lives, decay modes and relevant energies of the produced radionuclides and the problems they induce.

Corrosion product	Activation scheme	$T_{½}$	Decay mode and relevant energies (keV)	Problem related to the nuclide
Iron	^{54}Fe(n,γ)^{55}Fe	2.73 a	X-ray 5.9	Waste management
	^{58}Fe(n,γ)^{59}Fe	44.5 d	β^-: 466,274 γ:1099, 1292	Radiation build up
	^{54}Fe(n,p)^{54}Mn	312.2 d	γ: 835	Radiation build up
Nickel	^{58}Ni(n,p)^{58}Co	70.9 d	β^+: 1496 γ:811	Radiation build up
	^{62}Ni(n,γ)^{63}Ni	100 a	β^-: 67	Waste management
Cobalt	^{59}Co(n,γ)^{60}Co	5.27 a	β^-: 318 γ:1173, 1332	Radiation build up Waste management
Zinc	^{64}Zn(n,γ)^{65}Zn	244.3 d	γ: 1115	Radiation build up
Chromium	^{50}Cr(n,γ)^{51}Cr	27.7 d	γ: 320	Radiation build up

The activation products may be soluble, insoluble or bound to insoluble particles, and they are moved by the coolant solution all over the primary circuit. Activation products may be deposited on the surfaces of the primary circuit piping, resulting in elevated radiation fields away from the reactor and increased radiation burdens of maintenance workers (radiation build up). The main contribution to the radiation burden comes from nuclides with high γ-energies: $^{60,\ 58}$Co, ^{65}Zn, ^{65}Mn and ^{59}Fe. Nuclides ^{55}Fe, ^{63}Ni and ^{60}Co with longer half-lives are of more concern in the radioactive waste disposal. These same nuclides are also accumulated to metal parts of the core and the reactor vessel due to the intense neutron flux of the reactor. When reactors are decommissioned, the activated metal parts will be decontaminated by scrubbing and leaching with chemicals and the major part of the radioactivity will be released to waste disposal. With its long half-life, ^{63}Ni (100 a) will be the major source of radioactivity about 20 years after shut down of a nuclear reactor (figure 7).

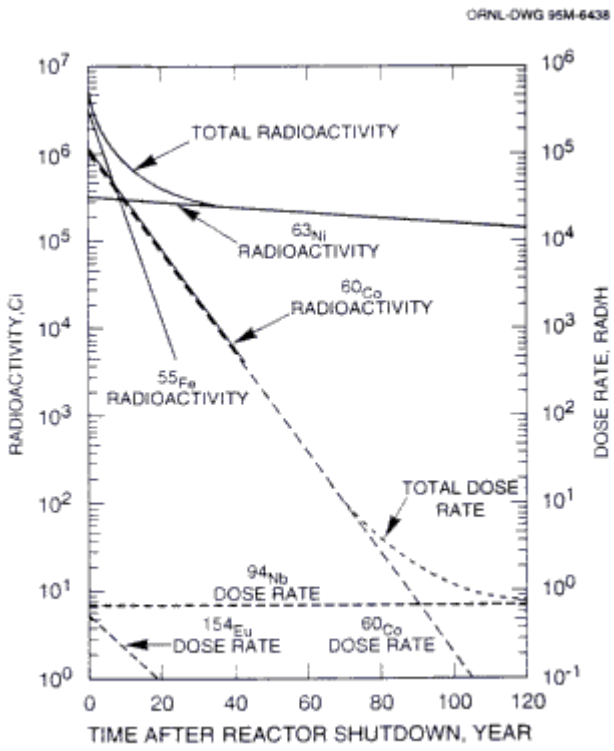

Figure 7. Dependence of radioactivity and dose rate in a boiling-water reactor core shroud after 40 years of operation.[63]

^{137}Cs and ^{90}Sr, which are produced by the fission of uranium in a nuclear reactor, were included in this study as the most important **fission products.** The yield of these nuclides is great relative to that of the activation nuclides, but they are normally retained inside the fuel rod at NPP, and released only in the event of fuel cladding failure or at the reprocessing plant when the fuel rod is chopped and dissolved. Also the **transuranium elements**, produced by neutron bombardment of uranium, are released at the fuel reprocessing plant. Small amounts of these actinides remain in the secondary waste solution (e.g. solvent wash, scrubbing solutions) of the Purex process (Plutonium Uranium Redox Extraction), which must be treated before release to the environment. The long half-life and toxicity (both chemical and radiation) of these elements makes them of great interest and, accordingly, plutonium and americium were also included in the study.

1.5 Theory for ion exchange studies

An ion exchanger is an insoluble material that has ionogenic groups to which counter ions can be bound (IUPAC). At its simplest, in binary exchange, when an ion exchanger with the exchangeable ion M^{Z_M} is contacting a solution containing ions N^{Z_N}, the exchange process can be written as

$$z_M N^{Z_N} + z_N \overline{M}^{Z_M} \quad \rightleftarrows \quad z_M \overline{N}^{Z_N} + z_N M^{Z_M} \tag{5}$$

where the barred symbols refer to the ions in the ion exchanger and z_M and z_N are the respective ion charges. The exchange is stoichiometric so that charge neutrality is retained both in the solution and in the ion exchanger. When more than two ions are introduced to the solution the system becomes multicomponent and the prediction of equilibrium becomes progressively complicated.

The selectivity of inorganic ion exchangers has been explained in a great many ways, but no unified hypothesis has been offered. In general, it can be stated that selectivity is a characteristic for all ion exchangers, but it varies with the experimental conditions. The selectivity of an exchanger is affected by factors such as physical characteristics/limitations and loading of the exchanger, electrical interactions between ion and exchanger and the nature of the exchanging ion and its speciation in the surrounding solution. The selectivity coefficient $k_{N/M}$ for the binary ion exchange process mentioned above can be defined as

$$k_{N/M} = \frac{\left[\overline{N}\right]^{Z_M}}{[N]^{Z_M}} \frac{[M]^{Z_N}}{\left[\overline{M}\right]^{Z_N}} \tag{6}$$

where $[\overline{N}]$,$[\overline{M}]$ refer to the equilibrium ion concentration in the exchanger and $[N]$,$[M]$ to that in solution. In cases where N is present in trace concentrations ($[\overline{N}] << [\overline{M}]$ and $[N] << [M]$), the concentration of M in the exchanger ($[\overline{M}]$) remains practically the same and can be considered equal to the ion exchange capacity (Q) of the exchanger. Theoretical specific capacity of the ion exchanger is the amount of charged sites (ionogenic groups) per gramme of exchanger (meq/g). Another widely used term is

practical capacity, (Q_p), which describes how many ions can be exchanged under specific conditions. This can be calculated in several ways, for example in column experiments it is the integral of the breakthrough curve.

The distribution coefficient (K_d) describes the distribution of ions between the external solution and the ion exchanger ($K_d = [\overline{N}] / [N]$) and is used to describe the exchanger affinity for a specific ion under given conditions. Inserting the ion exchange capacity (Q) and distribution coefficient (K_d) into equation 6 gives

$$k_{N/M} = K_d^{z_M} * \frac{[M]^{z_N}}{[Q]^{z_N}} \qquad (7)$$

If the K_d measurements are done with dilute solutions (<0.1 M) and the ions ([*N*]) are present in trace concentrations (as in most nuclear waste solutions), K_d depends only on the selectivity of the ion exchanger and the concentration of the macro ion ([*M*]) (i.e. the selectivity coefficient is practically independent of the ionic strength and no activity correction is needed). The K_d can be written as

$$K_d^{z_M} = k_{N/M} * \frac{[Q]^{z_N}}{[M]^{z_N}} \qquad (8)$$

Usually a logarithm is taken of this, giving equation 9, which is used to define the ion exchange process.

$$\log K_d = (1/z_M) \log (k_{N/M} * Q^{z_N}) - (z_N/z_M) \log [M] \qquad (9)$$

In an ideal ion exchange reaction, the plot of $\log(K_d)$ as a function of $\log([M])$ generates a straight line, the slope of which is the quotient of the valences of the exchanging ions.

It needs to be noted that certain chemical and physical events, commonly associated with dilute solutions, may cause erroneous interpretation of the ion exchange process. A major problem for some inorganic ion exchangers is that they disintegrate as small colloids in dilute solution, i.e. they peptize. Since the colloids act in a similar manner to

the ion exchanger, some of the exchanged ions are transferred into the solution (as colloids). The colloids are difficult to separate from solution by normal filtration and centrifugation, and they are usually retained in the solution phase. This causes erroneous K_d values and shifts the levels of metal breakthrough curves in column experiments. Peptization can be seen especially well in work with radioactive tracers since they can be measured in very small concentrations.

A serious source of error of chemical origin is hydrolysis of the exchanger. Weakly acidic ion exchangers, like zeolites and some metal oxides, may exchange their ions with hydronium ions (H_3O^+) in dilute solutions.

$$R\text{-}M^{Z_M} + 2\ H_2O \rightleftarrows R\text{-}H_3O^+ + OH^- + M^{Z_M} \qquad (10)$$

This will raise the pH of the solution (electroneutrality is maintained), which in turn can cause precipitation of hydrolysable ions, a change in their speciation, and dissolution of the exchanger. Increased solution pH as a result of hydrolysis can have two different effects on the measured K_d values. First, the K_d value may be increased by precipitation of the ion as solid hydroxide, and reducing its concentration in the solution. Second, K_d may be decreased or increased by change in the speciation of the exchanging ions. Hydrolysis is especially troublesome in batch experiments, where the solution volumes tend to be relatively small and, consequently, the changes in pH may be large. Another problem is that considerable conversion of exchanger to H_3O^+ form can take place, which may interfere with the interpretation of the binary (N/M) exchange equilibrium.

1.6 Scope

The objective of this study was to develop an effective inorganic ion exchanger for the separation of activated corrosion products from waste solutions. Special attention was paid to ^{63}Ni, which has been little studied even though it has a reasonably long half-life (100 a) and will be the major source of radioactivity in activated corrosion products after 20 years down the road from decommissioning of nuclear reactors (figure 7). The media from which these activated corrosion products will need to be separated most probably will be acidic solutions after decommissioning and decontamination of nuclear

reactors, and radioactive waste solutions with high concentration of inactive ions. Separating activated corrosion products from such a diverse group of solutions with a single exchanger would be difficult, and a group of materials was sought instead. The fission products caesium and strontium were included in the experiments in view of their great significance in nuclear waste management, however, they were not prime targets of the work.

One potential and highly interesting group of ion exchangers is tin antimonates, which are reported to have good chemical and physical stability and promising ion exchange properties.[42,64-77] As a means of exploring their possibilities, an extensive series of tin antimonates with a degree of Sn/Sb substitution from 0% to 100% was synthesised in a manner that would allow direct comparison of their structures and ion exchange properties. Also of interest was to find a relation between the metal uptakes of Ni and Co, so that Ni uptake could be predicted from the more abundant Co uptake data in the literature.

Lack of physical suitability has been a decisive obstacle in the column and commercial use of many promising inorganic materials. Particularly the lack of granular form and leaching of the material have been a problem. Evaluating the suitability of the synthesised tin antimonates for dynamic column experiments was considered important and was explored.

In addition, the potential of natural mica minerals for the separation of activated corrosion products was explored. Three different mica minerals were tested for their ion exchange properties both in their natural form, where potassium was the exchangeable cation, and in the sodium converted form.

2. Experimental

2.1 Synthesis of Sn / Sb metal oxides

Homogeneous products synthesised under identical conditions were the goal in the synthesis of tin-substituted antimony oxides and antimony-substituted tin oxides (tin antimonates). As a means of obtaining homogenous distribution of elements in product material, simultaneous precipitation of Sn and Sb from solution phase was chosen over the more commonly used procedures of prehydrolysation and mixing of separately precipitated oxides.

The synthesis, in brief, was as follows: tin antimonates were precipitated from acidic (6 M HCl) metal chloride (0.1 M, $SnCl_4$ and $SbCl_5$) solution by raising the pH of the solution with concentrated NH_3 solution. Synthesis time was kept short – 15 minutes of stirring after the precipitation and before liquid/solid separation – to obtain products of low ordering and crystallinity. Low crystallinity of the product material and pH 2 in the synthesis procedure were favoured in view of their probable positive effects on the ion exchange properties of the material.[70] The synthesis is described in detail in **I**.

2.2 Modification of mica minerals

Muscovite and biotite obtained from geological sites were crushed into small pieces with a hammer crusher and sieved to below 71 μm. Phlogopite, a mining product from the Kemira company, was obtained as 40 μm particles. Part of the minerals was converted from its natural potassium form into sodium form by two different procedures: by sequential shaking and by use of a fluidised-bed column as described in **V**.

2.3 Characterisation

The structures of the ion exchangers were characterised by powder X-ray diffraction (XRD), using a Phillips PW 1710 powder diffractometer (operating at 30 kV and 50 mA) with Cu K_α (1.54 Å) radiation. The elemental analysis of the tin antimonates was

carried out by X-ray fluorescence (XRF) using an Amptek 7 mm^2 Si(Li) XR-100CR detector and ^{241}Am excitation source. Thermogravimetric (TG) analyses were performed with a Mettler Toledo TA8000 system equipped with a TGA 850 thermobalance at a heating rate of 10°C/min under nitrogen atmosphere.

Atomic absorption spectrometry (AAS) was used for measurement of potassium in the conversion of the mica minerals to sodium form.

2.4 Ion exchange studies

The prime objective of the study was to find materials effective for the capture of activated corrosion products. Uptake of nickel and cobalt were of particular interest. In addition, the uptake properties for two of the major fission products (Cs and Sr) and two of the actinides (Pu and Am) were investigated. Several radioactive tracers were used in the study (table 2).

Table 2. Radioactive tracers used in the study, their decay modes and energies, half-lives, and source when present in radioactive wastes.[78]

Tracer	Decay mode and energy	Half-life ($T_{½}$)	Source
^{63}Ni	β^-, 67 keV	100.1 a	Activated corrosion product
$^{57}Co/^{60}Co$	γ, 122 keV / γ, 1173 and 1332 keV	271.8 d / 5.27a	Activated corrosion product
^{85}Sr	γ, 514 keV	64.8 d	Fission product
^{134}Cs	γ, 605 keV	2.06 a	Fission product
^{236}Pu	α, 5.77 MeV	2.85 a	Fuel activation
^{241}Am	γ, 59.5 keV	432.2 a	Fuel activation

Batch and column experiments were applied for determination of the ion exchange properties of the materials. The **batch experiments** were intended to produce primary ion exchange data such as distribution coefficients (K_d) and to demonstrate the effect of pH and competing ions on the radionuclide uptake. A small amount of finely ground, solid exchanger material (typically 25 or 80 mg) was placed in a vial with test solution (typically 10 ml) spiked with radionuclides. The samples were mixed in a rotary mixer till the solid/solution system obtained equilibrium (from 1 to 3 days). Centrifuging was applied for the separation of the different phases. Different centrifuge techniques were applied for the tin antimonates (3000 g for 10 min) and the mica minerals (63000 g for 30 min) owing to their dissimilar physical properties (**I**, **V**). Additional filtration was

applied for the tin antimonates to ensure the separation, while ultra centrifuging was sufficient for total separation of mica minerals from the solution. Distribution coefficients (K_d values) were calculated from batch experiments in the following way:

$$K_d = \frac{[\overline{N}]}{[N]} = \frac{(A_i - A_{eq})}{(A_{eq})} * \frac{V}{m} \qquad (11)$$

where $[\overline{N}]$ and $[N]$ are the concentrations in the exchanger and the solution, respectively. A_i is the activity of the tracer initially in the solution and A_{eq} is the activity of the tracer in the equilibrated solution after phase separation. V is the volume of the solution and m is the mass of the solid material. The activity of the tracers was measured with several different radioactivity detectors: the Wallac 1480 Wizard 3" Na(I) automatic gamma counter and Canberra ultra pure GC 4519 Ge-detector were used for γ-emitting nuclides, the liquid scintillation, LKB Wallac 1217 Rackbeta, was used for β-emitting ^{63}Ni and the Wallac 1220 Quantulus was used for α-emitting ^{236}Pu.

Column experiments were applied mainly to determine the physical applicability and suitability of the materials for ion exchange under dynamic conditions. The experiments were done in mini-columns through which solutions were pumped with a constant flow of about 20 or 30 bed volumes per hour (BV/h) (**III**, **IV**). The effluent was collected in suitable fraction sizes, in which the tracer content was measured with suitable radioactivity detectors as described above. The ion exchange properties of the materials were evaluated by calculating decontamination factors (DF) or breakthrough (BT) percentages for the materials.

$$DF = \frac{A_f}{A_o} \qquad (12)$$

$$BT = \frac{A_o}{A_f} * 100 \qquad (13)$$

where A_f is the column feed activity and A_o is the column outlet activity. BT percentage is more often used in the literature than DF, but DF illustrates the metal uptake more

realistically when the metal uptake is high (<< 1% BT). Also the pH of the effluent was measured.

2.5 Test solutions

Several solutions were used to test the ion exchange properties of tin antimonates. All the solutions were prepared from analytical grade chemicals and only nitrates were used. 0.1 M HNO_3 solution was used for collection of basic binary ion exchange data, while calcium nitrate solutions (0.1 M and 0.01 M) were used to simulate conditions with competing ions. Also, two simulates of floor drain water (FDW) were prepared. The FDW solutions were crude simulates containing only the most important and abundant ions that interfere with metal uptake of the ion exchange materials (100 ppm Na^+, 0.7 ppm Mg^{2+} and 1.5/15 ppm Ca^{2+}). FDW 2 solution, with ten-fold Ca^{2+} concentration relative to FDW 1, was intended to simulate a type of FDW very difficult to treat by ion exchange; for among the most common ions (Na^+, K^+, Ca^{2+}, Mg^{2+}), calcium interferes most heavily with the operation of antimonate ion exchangers.[68,79-80]
The concentrations of the tracer metals (^{57}Co, ^{63}Ni, ^{134}Cs and ^{85}Sr) varied slightly in the experiments but typically were on the order of 10^{-13} to 10^{-15} M. The speciation of the metals was calculated by the HydraQL program[81] and the metals were found to be almost entirely ionic (M^{2+} and M^+ for Cs) in all test solutions.
Actinides (^{236}Pu and ^{241}Am) were used in the same trace concentration as the other tracers although their speciation was not calculated.
In experiments with mica minerals the tracers were added to 0.1 M NaCl solution.

3. Results and discussion

The results of this work are discussed under two main headings: structure and ion exchange properties of the materials.

3.1 Structure of materials

3.1.1 Tin antimonates

Pyrochlore antimony pentoxide and rutile tin dioxide were precipitated when pure $Sb(V)Cl_5$ and $Sn(IV)Cl_4$ precursors were used in separate syntheses. Use of a mixture of these precursors resulted in the precipitation of metal oxides that could be divided into three groups on the basis of structure: materials with pyrochlore structure, materials with rutile structure and mixed metal oxides including both structures.

Table 3. Essential data for the synthesised tin antimonates. The contents of Sn and Sb are given as metal percentage and the water content as mass percentage of the products.

Sample code and starting reagents	Product Sn:Sb content (%)	Product structure	Water content at 110°C (%)
P_1: 0.1 M $SbCl_5$	100% Sb	Pyrochlore	3.7
P_2: 100 ml $SnCl_4$ +900 ml $SbCl_5$ (*)	79% Sb, 21%Sn	Pyrochlore, low crystallinity	2.1
A_1: 50 ml $SnCl_4$ +100 ml $SbCl_5$	66% Sb, 34% Sn	Amorphous	3.8
P_3: 250 ml $SnCl_4$ +500 ml $SbCl_5$	62% Sb, 38% Sn	Pyrochlore, poor crystallinity	5.3
A_2: 50 ml $SnCl_4$ +100 ml $SbCl_5$	58% Sb, 42% Sn	Amorphous	5.7
A_3: 200 ml $SnCl_4$ +300 ml $SbCl_5$ (**)	54%Sb, 46% Sn	Amorphous	6.2
A_4: 400 ml $SnCl_4$ +600 ml $SbCl_5$	54%Sb, 46% Sn	Amorphous, traces of pyrochlore	5.7
A_5: 250 ml $SnCl_4$ +250 ml $SbCl_5$	37% Sb, 63% Sn	Amorphous	6
R_1: 500 ml $SnCl_4$ +500 ml $SbCl_5$	33%Sb, 67% Sn	Amorphous/nano-crystalline rutile	4.4
R_2: 1000 ml $SnCl_4$ +500 ml $SbCl_5$	17% Sb, 83% Sn	Nanocrystalline rutile	5.1
R_3: 1000 ml $SnCl_4$ +100 ml $SbCl_5$ (***)	7% Sb, 93% Sn	Nanocrystalline rutile	6.6
R_4: 0.1 M $SnCl_4$	100% Sn	Nanocrystalline rutile	5.2

Secondary sample codes: * SnSbP, ** SnSbMOX, ***SnSbR

A tendency towards the formation of rutile structure was observed in the tin antimonate synthesis. This was seen as higher tin ratio in the products than in the starting reagents

(table 3). Physical characteristics of the Sb and Sn ions may explain this, since Sb^{5+} ions are slightly smaller than Sn^{4+} ions (r 0.60 and 0.69 Å in sixfold co-ordination, respectively)[82]. The smaller ion size of Sb^{5+} allows it to fit more easily in the lattice of tin dioxide than does Sn^{4+} in the lattice of antimony pentoxide.[83]

The structure of the pyrochlore materials was similar to the structure of antimony pentoxide (space group Fd3m) up to tin substitution of ~35%. Gradual addition of tin to the material resulted in lower intensity and broader peak size in XRD diffractograms indicating lower crystallinity and smaller crystal size (figure 8). The most intense peaks of the antimony pentoxide structure were still recognisable in XRD diffractograms of materials with up to 38% Sn content. The crystal size of the materials decreased from roughly 160 nm to 25 nm with progressive Sn for Sb substitution, as calculated with Phillips software for the (111) peak.

The rutile structure was identified as a solid solution of tin dioxide (space group $P4_2/mnm$), with antimony substitution up to ~35%. The nano-crystalline character of the tin dioxide meant that possible changes in the structure with antimony substitution were almost impossible to detect with the available XRD apparatus. Fortunately, the structure of tin dioxide has been widely studied owing to its properties of transparency and semi-conductivity, which are valuable in optoelectronic devices.[84-87] These studies have shown that as much as 40% of tin can be replaced by antimony, and that antimony occupies the sites of tin in the crystal lattice of rutile tin dioxide. Higher antimony content in the synthesis solutions would result in the precipitation of the antimony pentoxide phase.[83,84,88]

Materials in the region between 35% to 65% metal substitution were also difficult to characterize on the basis of XRD measurements because of their amorphous character. Most likely these materials were agglomerated mixtures of two metal oxides at various levels of Sn or Sb substitution, formed in competition between the pyrochlore and rutile structures. Only an indication of a possible change in the material structure of the majority of oxides within the product could be deduced from changes in the XRD diffractograms. For example, the most intense XRD reflections (110 and 101) of nano-crystalline tin dioxide were two broad peaks, before and after 30 2θ/degrees (figure 8). When antimony was added to the synthesis, the intensity of these broad peaks decreased and with ~60% antimony content the peaks merged into a single broad peak just before

30 2θ/degrees where the two intense XRD reflections (311 and 222) of antimony pentoxide are located.

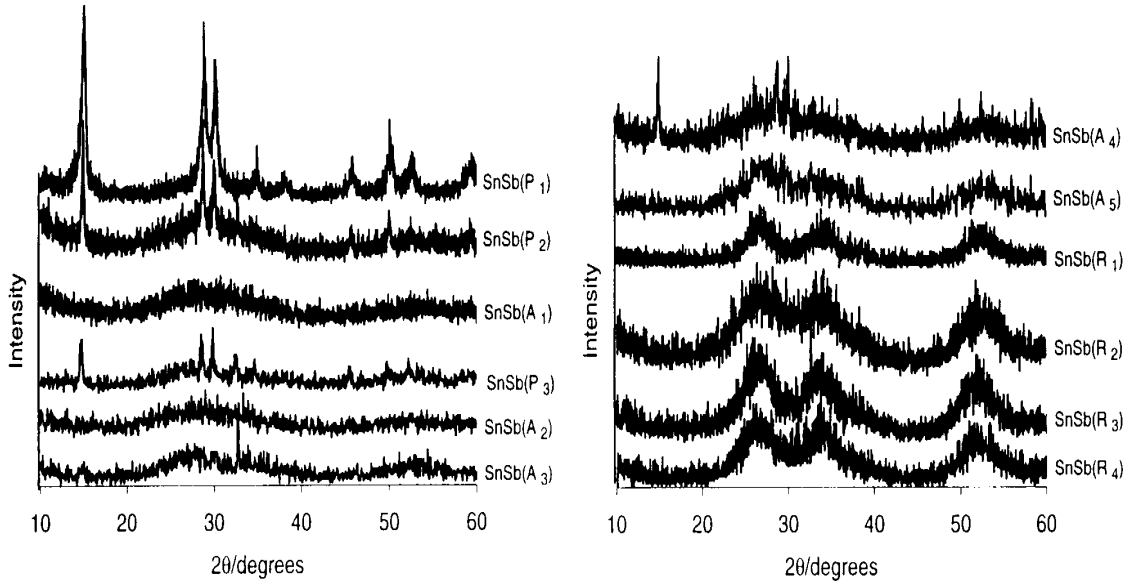

Figure 8. Selected XRD diffractogram patterns of tin antimonates used in the study (**III**). See table 3 for sample codes.

Thermogravimetric (TG) measurements gave additional information, which was particularly important for the characterization of mixed metal oxide tin antimonates with amorphous-like XRD diffractograms. Thermograms of pure antimony and tin oxides were typical of those of particle hydrates (SnO_2) with continual water release and of framework hydrates (Sb_2O_5) with more specific water release (figure 9). Sn for Sb substitution of pyrochlore Sb_2O_5 generated a second 'peak' in the DTA (differential thermal analysis) graph at ~200°C, in addition to the peak characteristic of water release of crystalline Sb_2O_5 just before 400°C.[42] This second DTA peak persisted with increasing Sn for Sb substitution, from pyrochlore to mixed metal oxide materials with up to 50% tin content. The DTA curve of tin antimonate with 54% Sn content gave only a small peak at ~400°C and no peak at all at ~200°C; and materials with higher Sn content gave no peak at ~400°C either (figure 9). The presence of these two peaks, particularly the ~400°C peak, offered further evidence of the presence of the pyrochlore phase in mixed metal oxide materials that produced more or less amorphous XRD patterns. Together the XRD and TG data suggest that the mixed metal oxides with less than 50% tin content had high pyrochlore content with low crystal ordering.

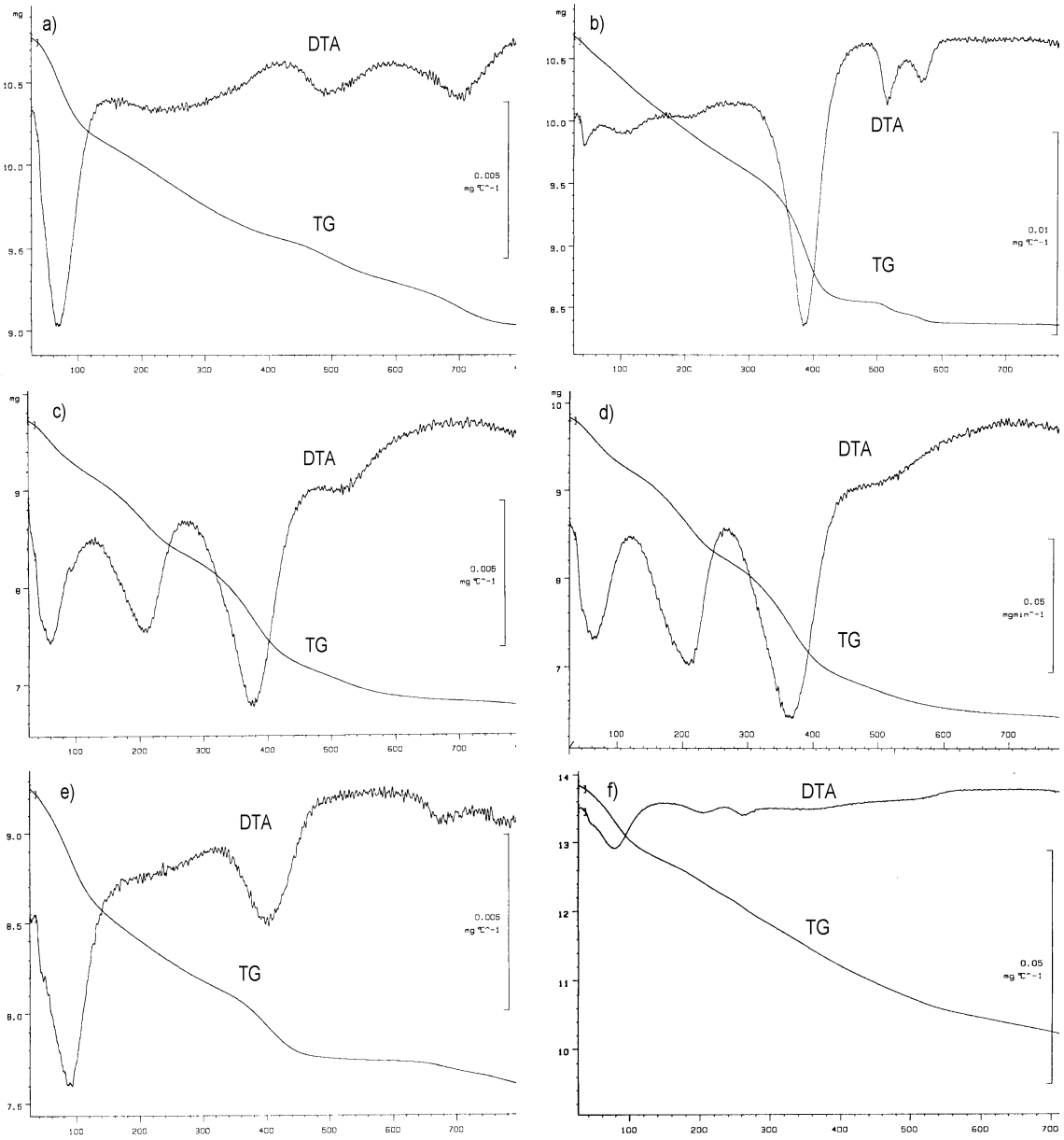

Figure 9. Thermogravimetric curves measured for synthesised a) rutile tin dioxide, b) pyrochlore antimony pentoxide, c) 38% Sn content tin antimonate (P_3), d) 46% Sn content tin antimonate (A_4), e) 54% Sn content, and f) 93% Sn content (R_3). Temperature on the x-axis and mass of the material on the y-axis. The TG curve presents the weight loss of the material and the DTA curve the endothermicity (downward) of the weight loss.

It was of interest to investigate the effect of higher synthesis pH of tin antimonates on their material structure and ion exchange properties. Higher synthesis pH (relative to the pH 2 normally used) resulted in higher Sn content in the product. Increasing the synthesis pH by ~4 units increased the Sn content of the product by 5% and 15%, respectively, when 1Sb:2Sn and 2Sb:1Sn were the ratios of the starting reagent, in otherwise identical syntheses (table 4). In addition, higher synthesis pH decreased the

crystallinity of the tin antimonates (figure 10). This is in agreement with a report[42] that increased acidity of the synthesis will increase the crystallinity of the product.

Table 4. Synthesis data for selected tin antimonates

Sample code and starting reagents	Synthesis pH	Product Sn:Sb content (%)	Product structure
S6: 100 ml $SnCl_4$ +50 ml $SbCl_5$	pH 2	80% Sn, 20%Sb	Nanocrystalline rutile
S7: 100 ml $SnCl_4$ +50 ml $SbCl_5$	pH 6.2	85% Sn, 15%Sb	Nanocrystalline rutile
S40: 50 ml $SnCl_4$ +100 ml $SbCl_5$	pH 2	47% Sn, 53%Sb	Amorphous
S40b: 50 ml $SnCl_4$ +100 ml $SbCl_5$	pH 6.5	61% Sn, 39%Sb	Amorphous

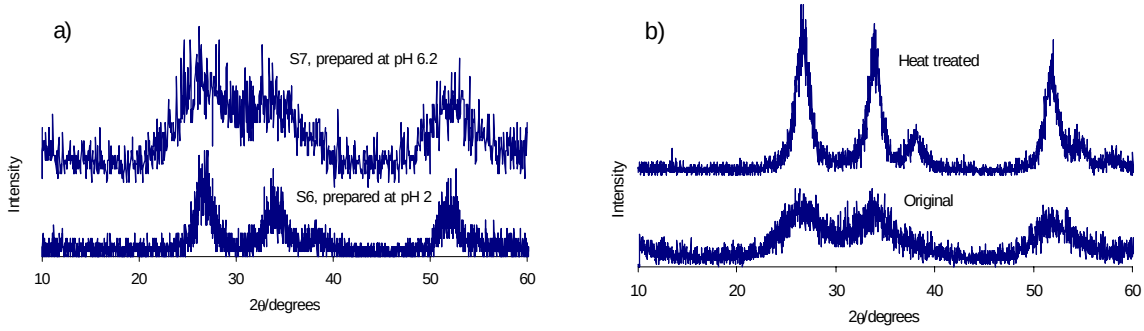

Figure 10. Effect of (a) synthesis pH and (b) heat treatment on crystallinity of the samples S7 and S6 (see table 4) (a) and tin dioxide (b).

Although low crystallinity products were preferred, the possibility of increasing the crystallinity in the product was tested by ageing of the material in the synthesis solution and by post-synthesis heat treatment. Ageing for three days did not produce any substantial increase in the crystallinity of the product. Heat treatment of 1 g of product for four hours at 430°C, on the other hand, increased the crystallinity of the products noticeably (see XRD patterns of tin dioxide in figure 10b).

3.1.2 Mica minerals

Conversion of mica minerals from their naturally occurring potassium form to sodium form was successful with biotite and phlogopite: the degree of conversion was close to 100%. Owing to the high aluminium content, the conversion of muscovite was only ~5%. The aluminium in the tetrahedral layer generates a relatively high negative

electrostatic charge on the surfaces of the three-layer units, which retards diffusion of the bulky (K^+) interlayer cations.

The degree of conversion was calculated from the potassium content of the effluent from the fluidised bed 'converter', but the conversion can also be seen in the measured XRD diffractograms. Since sodium-form mica minerals are hydrated, the potassium and sodium forms are readily distinguished by their XRD diffractograms. The strongest reflection of nonhydrated mica minerals typically lies at ~9° 2θ/degrees, which corresponds to interplanar spacing of 10 Å.[89] In the case of hydrated micas the corresponding values are ~6° 2θ/degrees and about 15 Å (figure 11).[90] As seen from the XRD diffractograms, phlogopite and biotite were almost entirely, while muscovite was only partially converted to sodium form.

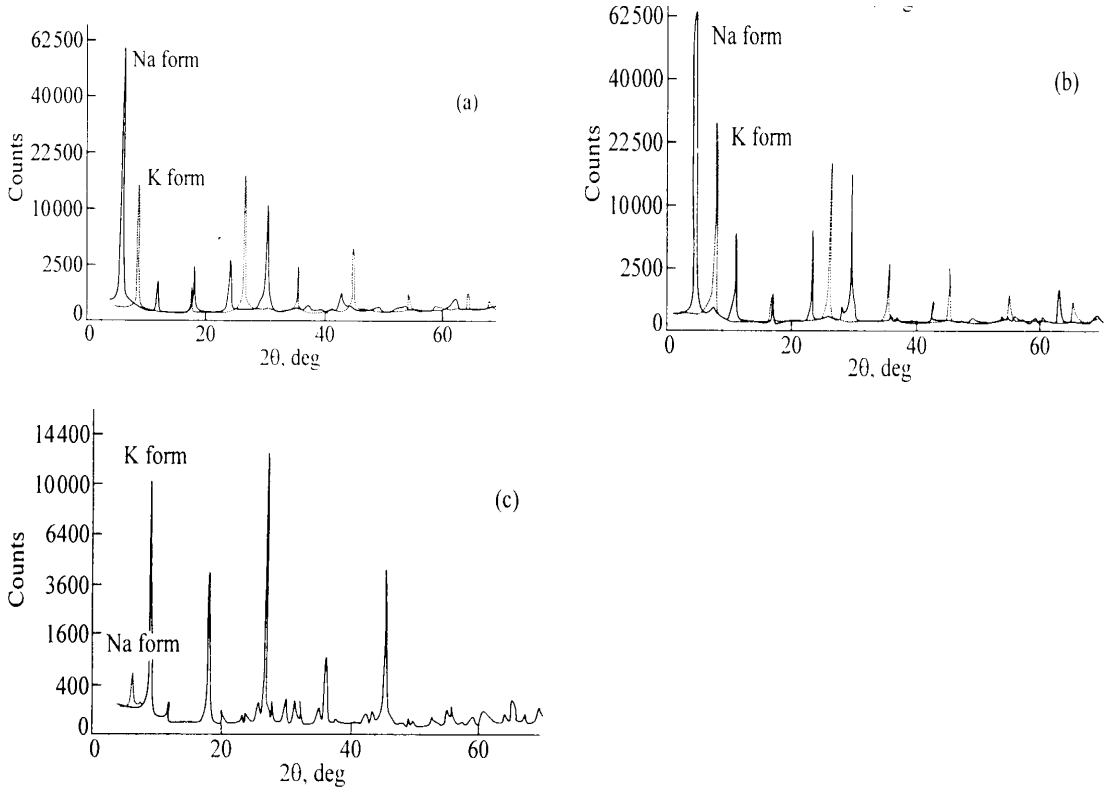

Figure 11. XRD diffractograms of the potassium- and sodium-form mica minerals: a) phlogopite, b) biotite and c) muscovite (**V**).

3.2 Ion exchange studies on tin antimonates

Substitution of metals in metal oxides can have several effects on the ion exchange properties of the material. The initial assumption of our study was that substitution of

one metal by a more electronegative one would increase the acidity of the oxide and in that way improve the ion exchange properties of the material in acidic solutions. Substitution could also have an effect on the framework structure of the material, and thereby change the selectivity and the diffusion rate within the tunnels or cavities of the material. The tin antimonates fell into the same three categories on the basis of their ion exchange properties as on the basis of their structure.

3.2.1 Pyrochlore-structured tin antimonates

The rigid three-dimensional structure of pyrochlore antimony pentoxide has a tunnel structure with openings of 6 Å.[42] The ion exchange sites are located at the surface and, still more abundantly, inside the material in tunnels and cavities.[34] Since the opening of the tunnels is relatively small, most of the ion exchange sites are inaccessible to cations with large hydration shells and their uptake occurs mostly on the surface of the material. It has been noted, however, that some exchanger materials can strip away the hydration shell of certain metals, allowing the metals to enter the tunnels as partly hydrated ions.[34] The rigid three-dimensional structure of pyrochlore-structured materials changes only slightly upon conversion to different metal forms and with metal substitution in the lattice.[91] Progressive tin for antimony substitution in antimony pentoxide resulted in an increase in the lattice parameter (a) and in the K_d values of pyrochlore-structured materials (table 5, figure 12). Higher K_d values were attributed to easier access of the exchanging ions to the inner ion exchange sites (inside tunnels and cavities). Sharp increase in the K_d values was observed along with increase in the lattice parameter from 10.34 Å to 10.39 Å (from exchanger $SnSb(P_2)$ to (P_3)).

Table 5. The most intensive XRD reflections and mean lattice constants (a) of the pyrochlore-structured materials, and K_d values (ml g^{-1}) in 0.1 M HNO_3 solution for ^{57}Co and ^{63}Ni. For sample codes see table 3.

Sample	*hkl* (111), *d*/Å	*hkl* (311), *d*/Å	*hkl* (222), *d*/Å	Mean lattice constant (a), Å	K_d value, ml/g (Co/Ni)
$SnSb(P_1)$	5.893	3.110	2.972	10.272	19,300 / 850
$SnSb(P_2)$	5.968	3.122	2.983	10.342	20,800 / 1,200
$SnSb(P_3)$	6.015	3.131	2.991	10.386	160,400 / 11,500
$SnSb(P_2)$ Ca-form	5.928	3.097	2.964	10.269	

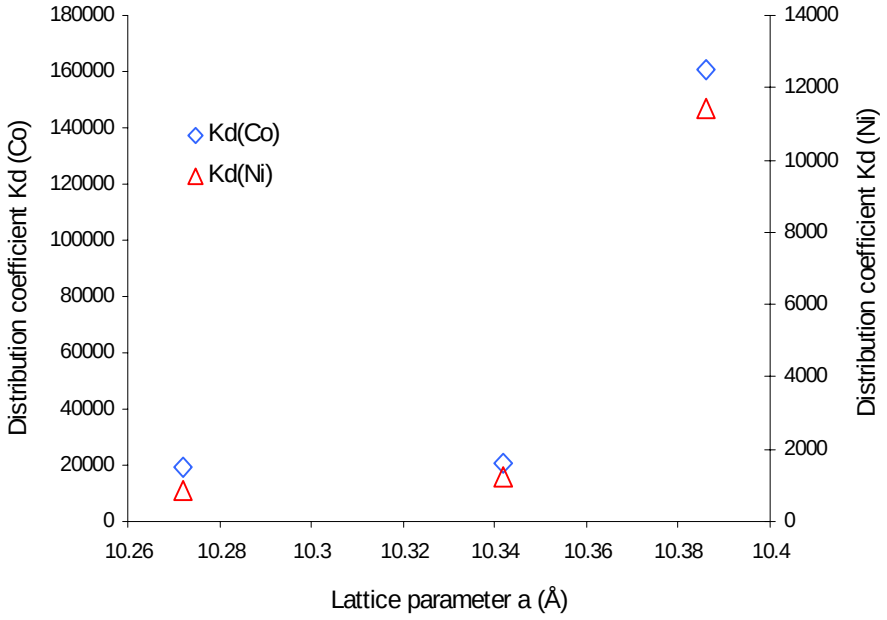

Figure12. Distribution coefficients (ml/g) of ^{57}Co and ^{63}Ni in 0.1 M HNO_3 solution as a function of the lattice parameter of $SnSb(P_2)$ with pyrochlore structure (**IV**).

3.2.2 Rutile-structured tin antimonates

As a consequence of the small crystal size and particle hydrate character of rutile-structured tin antimonates, electrostatic attraction governed the ion exchange properties of these materials. Ion exchange in these materials occurs mainly on the surfaces and since the exchanging ions encounter little or no steric interference, the electrostatic forces between the exchanging ions and exchange sites control the exchange. The point of zero charge (p.z.c.) of tin dioxide is rather high (pH ~4) considerably limiting the use of the material for cation exchange purposes in acidic conditions (p.z.c. is the pH below which the OH groups cannot deprotonate and cation exchange cannot occur, equation 1).[67,92] Substitution of Sb for Sn in the lattice of tin dioxide decreased the p.z.c. of the materials, as observed in the increase in the metal uptake from 0.1 M HNO_3 solution of material with less than ~80% Sn content (figure 13). The highest K_d values were observed with materials of 63% Sn content, which is near the highest reported[88] level of substitution (40%) of Sb into the lattice of rutile SnO_2.

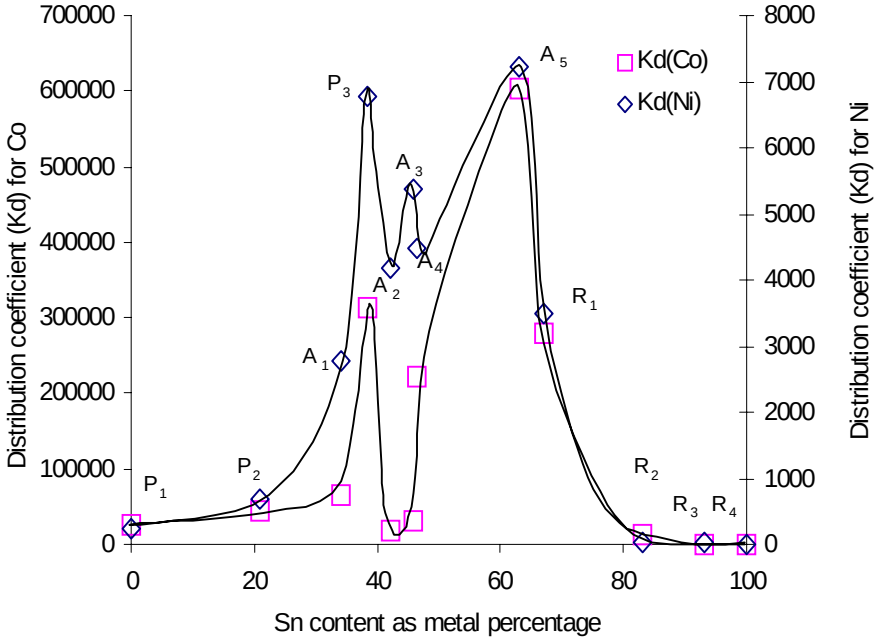

Figure 13. Distribution coefficients (ml g^{-1}) for ^{57}Co (□) and ^{63}Ni (◊) in 0.1 M HNO_3 solutions as a function of Sn content (in metal %)(**IV**). For sample codes see table 3.

3.2.3 Mixed metal oxides of tin and antimony

K_d values for the mixed metal oxide tin antimonates varied widely (figure 13). For example, from 0.1 M HNO_3 solution the cobalt uptake was much higher $SnSb(A_4)$ than on $SnSb(A_3)$ though Sn content was 46% in both. The synthesis of the two exchangers was identical, but the XRD pattern obtained from the $SnSb(A_4)$ exchanger showed traces of pyrochlore reflections, while the XRD pattern of the $SnSb(A_3)$ exchanger was amorphous-like, indicating less ordered crystal structure. The DTA curves for the two materials were identical, suggesting their similar structure. On the basis of the XRD and DTA data, the structures of the $SnSb(A_3)$ and (A_4) exchangers were thus considered to be the same except for the higher crystal ordering of the $SnSb(A_4)$ exchanger. As a consequence of the lower ordering of the $SnSb(A_3)$ exchanger, its tunnel structure was probably distorted, hindering the ion exchange from deep inside the material.

3.2.4 Uptake of activated corrosion products

The uptake on tin antimonates of activated corrosion products from different test solutions was most promising, but it was noted that the uptake of cobalt (^{57}Co) was at

considerably higher level than the uptake of nickel (^{63}Ni). Although the K_d values of Co and Ni were at different levels, the values, nevertheless, changed in almost parallel fashion for the rutile-structured materials and in closely similar fashion for the pyrochlore-structured materials. The relation between the K_d values for Co and Ni on the same tin antimonate varied most with the mixed metal oxide materials, particularly with materials of amorphous structure.

Physical properties of the exchanging ions and steric hindrance of the exchangers were considered as the most probable reasons for the differences in metal selectivity. The hydrated ion radii of cobalt and nickel are 2.95 and 3.02 Å, respectively.[93] With its 6 Å tunnel size, the pyrochlore antimony pentoxide generates an ion sieve effect, which appears as a difference in metal uptake levels between the otherwise very similar metals. Progressive Sn for Sb substitution resulted in an increase in the lattice parameter (a) and increase in the K_d values of cubic, pyrochlore-structured materials (figure 12). Higher K_d values were associated with easier access of exchanging ions to the inner ion exchange sites (inside tunnels and cavities) of the materials. The K_d values rose sharply with the increase in the lattice parameter from 10.34 Å to 10.39 Å (from SnSb(P_2) to SnSb(P_3)): the K_d values increased 9.6-fold for nickel and 7.7-fold for cobalt. This level of increase was almost the same as observed in earlier experiments (figure 13), where the K_d values increased from SnSb(P_2) to SnSb(P_3) 9.8-fold for nickel and 7.3-fold for cobalt. Relative to SnSb(P_2), the exchanger SnSb(A_1), which in Sn content lies between SnSb(P_2) and SnSb(P_3) (figure 13), exhibited 4.0 times as great nickel uptake but only 1.5 times as great cobalt uptake, measured in K_d values. The smaller increase in K_d values of cobalt than of nickel may be related to the amorphous structure of SnSb(A_1). In the case of the pyrochlore-structured materials, most of the cobalt uptake is assumed to take place in tunnels and cavities, but most of the nickel uptake at the outer surfaces of the material owing to steric hindrance of the larger hydratation shell of the nickel ion. Since the SnSb(A_1) exchanger probably consists of small pyrochlore crystals with low ordering, which produce an amorphous XRD pattern, the pore structure of the material must be disordered restricting entrance and exchange of the ions deep inside the material. A similar difference in K_d values between nickel and cobalt can be seen for the exchangers SnSb(A_2), (A_3) and (A_4). The SnSb(A_4) exchanger has traces of pyrochlore structure in its XRD pattern, i.e. crystals are more ordered, producing more tunnelled structure and higher cobalt uptake (figure 13).

For the exchangers with rutile structure ((SnSb(R_1) to (R_4), figure 13), changes in uptakes of cobalt and nickel as a function of Sn content followed an almost identical pattern. This similarity in metal uptake is due to the particle hydrate structure of the rutile-exchangers, where the ion exchange can be presumed to take place at the material surfaces. When exchange takes place at the surface the differences in selectivity originating from the size of the exchanging cation are reduced and the effect of electrostatic attraction is emphasised.

3.2.5 Effects of pH and calcium ions on metal uptake

The pH dependence of the metal uptake is of importance in planning the decontamination of floor drain waters since the pH can easily be adjusted. Original and calcium-form SnSb(P_2) exchangers were tested for their Ni uptake from calcium-bearing solutions of different pH, but, unexpectedly, marked differences were not seen between the two exchanger forms. The uptake of nickel was only slightly lower for the Ca-form SnSb(P_2) exchanger than the original-form SnSb(P_2) exchanger (figure 14a). This may have to do with the batch conditions (0.01M $Ca(NO_3)_2$). Under these batch conditions, as much as half of the original-form exchanger could have converted to calcium form. Such change is known to decrease the lattice parameter of materials with pyrochlore structure[68], and decrease in the lattice parameter of calcium-form SnSb(P_2) was indeed observed (table 5). Possibly the outer edge crystals of the original SnSb(P_2) were changed into calcium form, decreasing the size of the opening of the tunnel structure and resulting in lower K_d values for nickel.

In view of the possible change in exchanger form in the test solution, also other tin antimonates of different structure were converted to calcium form before measurement of their metal uptake dependence on equilibrium pH. The K_d values of three tin antimonates – pyrochlore structure SnSb(P_2), rutile structure SnSb(R_3) and mixed metal oxide SnSb(A_3) – were measured as a function of pH (figure 14b). A small Sb for Sn substitution in the lattice of SnO_2 (SnSb(R_3)) induced cation exchange properties in the material, even at fairly low pH (~1.5). An increase in the dissociation of ion exchange groups of the SnSb(R_3) occurred at neutral pH and excellent K_d values of over 175 000 ml/g resulted. The SnSb(P_2) exchanger was the most affected by interfering Ca ions, and it had the lowest nickel uptake, although the K_d values in the most acidic conditions

were slightly higher than those of the $SnSb(R_3)$. Excellent nickel uptake was obtained with the $SnSb(A_3)$ exchanger from acidic solutions. The only explanation for the exceptionally high selectivity for nickel from 0.01 M $Ca(NO_3)_2$ solution at pH below 1 (figure 14b) would seem to be that the exchanger consisted mainly of pyrochlore antimony pentoxide with high degree of Sn/Sb substitution (see figure 13).

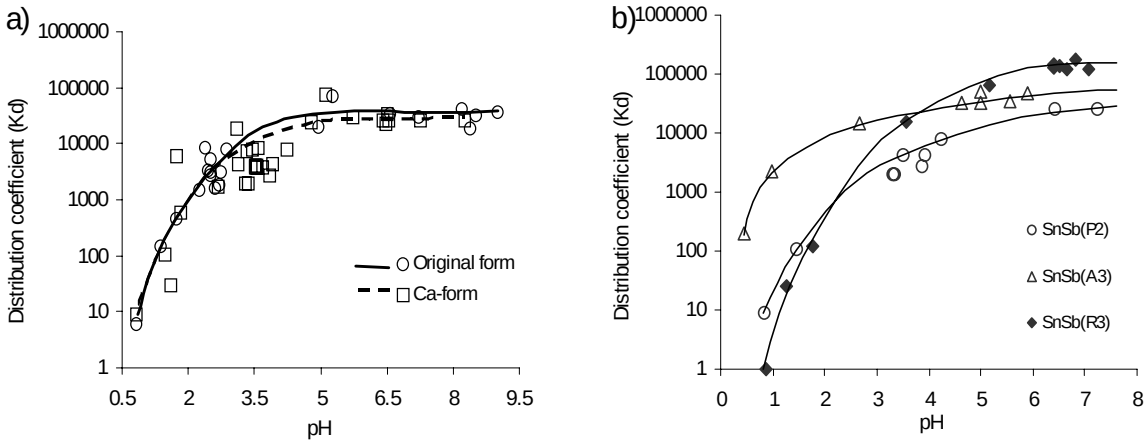

Figure 14. Distribution coefficients for uptake of nickel in 0.01 M $Ca(NO_3)_2$ solution onto (a) pyrochlore $SnSb(P_2)$ (**IV**) and (b) tin antimonates of different structure (**II**).

3.2.6 Column performance

Two objectives in the column experiments with tin antimonates were (1) to demonstrate their metal uptake performance and (2) to verify their physical suitability for dynamic column use (**III**,**IV**). The tin antimonates tested – pyrochlore with Sn content of 21% ($SnSb(P_2)$), mixed metal oxide (Sn 45.8%, $SnSb(A_3)$) and rutile (Sn 93.1%, $SnSb(R_3)$) – performed well in column conditions with one exception. Except with the solution of high calcium content, the materials retained their physical form and large volumes of solutions could be treated with good metal uptake performance. Column clogging was associated with the solution with high calcium content (15 ppm in FDW 2 solution, **III**) although clogging was not immediate and relatively large volumes, some 5000 bed volumes (BV), of solution were successfully treated. In particular, the $SnSb(A_3)$ exchanger became clogged in the FDW 2 solution. The structure of the $SnSb(A_3)$ exchanger was considered to be an agglomerated mixture of tin and antimony oxides with specific Sn/Sb substitutions in their lattices (**I** and **IV**). The pyrochlore structure of antimony pentoxide is known to peptize in dilute solutions, and if the pyrochlore

content of the $SnSb(A_3)$ exchanger had been peptized by the FDW 2 solution, a decrease in the decontamination factors (DF) should have been observed owing to the physicochemical properties of colloids (see above). Instead, the clogging usually occurred at fairly high DF level, suggesting a different origin for the column failures. Increased crystallisation of pyrochlore tin antimonate was observed when this was converted to calcium form (figure 15). This further ordering of the pyrochlore content could have broken the agglomerate form of the $SnSb(A_3)$ exchanger, resulting in the release of small particles of the material, and eventual clogging the column.

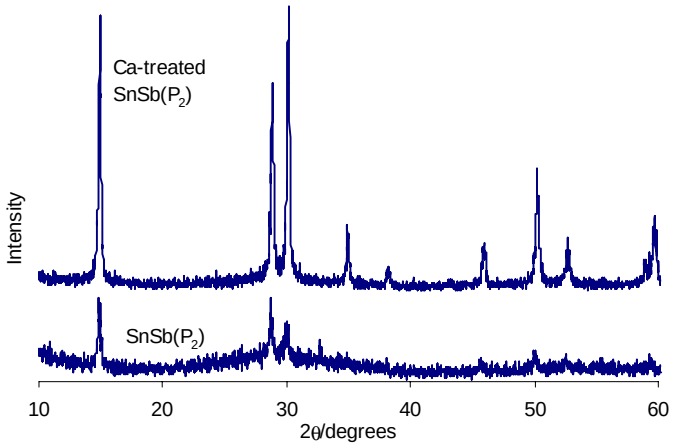

Figure 15. XRD diffractograms of normal and calcium-treated pyrochlore tin antimonate (**IV**).

The earlier batch experiments with tin antimonates indicated substantially higher cobalt uptake than nickel uptake (**I**,**II**). In the column experiments, however, uptake of the two metals on the $SnSb(A_3)$ exchanger was surprisingly similar. In addition, the reported[94] effect of pH on the selectivity sequence of tin antimonates was observed, and indeed the uptake on $SnSb(A_3)$ from FDW 1 solution was higher for nickel than cobalt (figure 16).

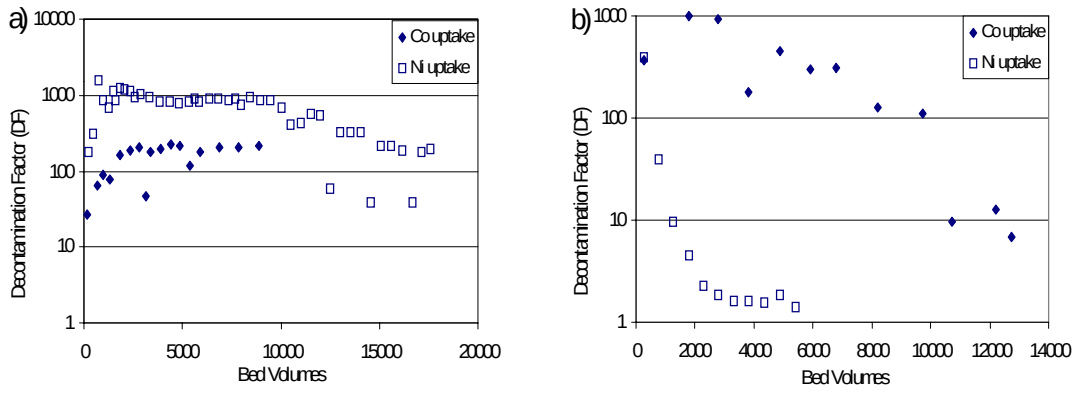

Figure 16. Nickel and cobalt uptake of the $SnSb(A_3)$ exchanger from a) calcium-bearing FDW 1 solution and b) from 0.1 M HNO_3 solution.

The different ion exchange sites of pyrochlore materials may explain the high nickel uptake. There are two types of ion exchange sites in pyrochlore materials: on the surface of the material and in tunnels and cavities inside the material. The latter are responsible for most of the ion exchange capacity of the materials.[28,34] The high uptake of cobalt in batch experiments may be associated with ion exchange inside the material, whereas the uptake of nickel takes place on outer surfaces of the material. The kinetic constraints of dynamic column experiments will favour metal uptake on the surfaces rather than inside the tunnels of the material, the surfaces being more favourable for nickel uptake than cobalt uptake. This preference was also evident in the column experiment done with the $SnSb(A_3)$ exchanger, where the two metals were in the same solution (0.01 M $Ca(NO_3)_2$, used to simulate neutral bond water) and the pH of the eluent was changed (figure 17). This experiment also demonstrated the change in the selectivity sequence with pH. In addition, the marked differences in the BT -levels of the metals suggest that nickel and cobalt might themselves be separated through variation in acid concentration of the eluent. This finding agrees with the reported enthalpies of the ion exchange reaction on crystalline antimony pentoxide ($\Delta H°$ of $M^{2+} \rightarrow H^+$ is 9.0, 79.5 and 159.1 kJ eq^{-1} for Ca, Ni and Co, respectively)[42].

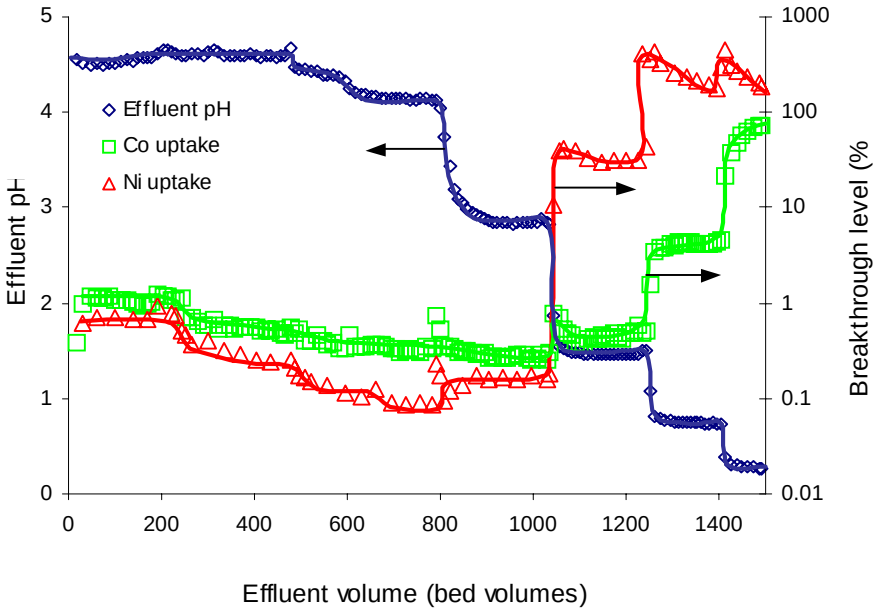

Figure 17. Breakthrough curves of ^{57}Co (□) and ^{63}Ni (Δ) for mixed metal oxide tin antimonate ($SnSb(A_3)$) in 0.01 M $Ca(NO_3)_2$ solution (**IV**).

3.2.7 Uptake of fission products

In view of the importance of the fission products in nuclear waste management, strontium and caesium were included in the experimental program. Since excellent ion exchangers for separation of these nuclides are already available, the uptake of Sr and Cs was tested only in column experiments (figure 18). The uptake of Sr from acidic solution (0.1 M HNO_3) was superb with tin antimonate of pyrochlore structure ($SnSb(P_2)$), and large volumes (> 25 000 BV) of this solution were treated with high decontamination factor (DF). The good Sr uptake of $SnSb(P_2)$ was expected since pyrochlore antimony pentoxide is well known for its Sr uptake. A suppressing effect of competing calcium ion (FDW solutions) on the Sr uptake was observed, but still the performance of mixed metal oxide ($SnSb(A_3)$) tin antimonate was outstanding. Comparison of the results of this experiment with the results for commercial sodium titanate exchanger (CoTreat®) showed very similar trends in Sr uptake for the two materials, but with tin antimonate the uptake continued slightly longer (**III**). The Sr uptake of tin antimonates was clearly related to the pyrochlore content of the material, since the third tin antimonate ($SnSb(R_3)$), with rutile structure, exhibited only modest Sr uptake.

Caesium uptake was modest on both the tin antimonates studied (figure 18b). Unlike cobalt and strontium, which are sorbed by chemical sorption, caesium uptake occurs by physical sorption.[95]

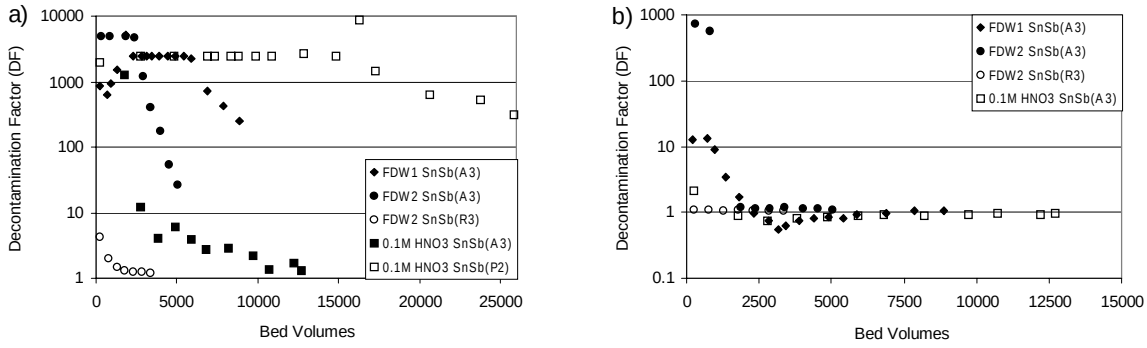

Figure 18. The uptake on tin antimonates of (a) strontium and (b) caesium from two calcium-bearing simulate solutions (FDW 1 and 2) and from 0.1 M HNO_3 solution (**III**).

3.2.8 Uptake of actinides

The uptake of actinides was tested in batch experiments in 0.1 M, 0.01 M and 0.001 M HNO_3 solutions. Distribution coefficients measured in these experiments were relatively high but also somewhat perplexing (table 6). The plutonium uptake increased with the acidity of the solution, which is in contradiction to the typical cation exchange process of the tin antimonate investigated ((SnSb(P_2), characterised as a weak cation exchanger). Study of the probable speciation of the plutonium in the solutions showed the plutonium uptake more or less follow the speciation curve of $Pu(III)(NO_3)^{2+}$, although the valence of plutonium should be +IV in these solutions.[96-97] The nitrate species of Pu(IV) did not correlate with the uptake trend. Likewise, the uptake of americium was hard to interpret. An extremely high K_d value was measured in 0.1 M HNO_3 and good K_d values in 1 M and 0.01 M HNO_3 solutions. The solution chemistry of actinides is highly complicated, especially with solids that may introduce redox potential to the system, and since the measured K_d values for both plutonium and americium were high, no further studies on actinide uptake were carried out.

Table 6. The K_d values of plutonium and americium for the SnSb(P_2) exchanger in nitric acid solutions.

Solution	K_d (Pu), ml/g	K_d (Am), ml/g
0.01 M HNO_3	6 170 ± 85	16 060 ± 84
0.1 M HNO_3	85 750 ± 3950	4 234 376 ± 1 839 000
1 M HNO_3	100 300 ± 7250	4 432 ± 16

3.3 Ion exchange studies on mica minerals

The conversion of mica minerals to sodium form had a noticeable effect on their metal uptake properties (table 7). In general, the conversion to sodium form increased the uptake of bivalent ions (Co and Sr) and decreased the uptake of univalent ion Cs, with the exception of the Cs uptake on phlogopite and the Co uptake on muscovite. Even the low conversion of muscovite (~5%) resulted in considerable changes in the metal uptake properties.

Conversion to sodium form had a positive effect on strontium uptake, but the K_d values were still fairly moderate for all the three mica minerals. The moderate strontium uptake was expected since only brittle micas, with high negative charge in the tetrahedral layer and alkaline earth as interlayer cation, are known for selective strontium uptake.

The uptake of the other fission nuclide, caesium, was good on potassium-form muscovite but dropped to one tenth of that value after conversion of the muscovite to sodium form. The same trend was seen in caesium uptake on biotite, but the impairing effect of the conversion was not so great. Only with phlogopite were the K_d values higher for the sodium than the potassium form, but this may have been due to higher equilibrium pH of the sodium than the potassium form.

High K_d values were obtained in cobalt uptake. Conversion to sodium form doubled the already high K_d values of phlogopite, and with biotite the increase was over tenfold. A decrease in cobalt uptake on muscovite was observed with the partial conversion to sodium form. The promising cobalt uptake of sodium-form phlogopite was also investigated as a function of pH. The effect of pH on the metal uptake was very strong, as is typical for weak acid cation exchangers. A steep increase in K_d values was observed above pH 7.2, and K_d values as high as 150 000 (ml/g) were obtained at pH 7.8 (figure 19).

Table 7. Distribution coefficients (K_d, ml/g) for uptake of ^{60}Co, ^{85}Sr and ^{134}Cs on natural and modified mica minerals from 0.1 M NaCl solution (**V**).

Mineral	K_d (^{60}Co) / (pH)	K_d (^{85}Sr) / (pH)	K_d (^{134}Cs) / (pH)
	Natural mica minerals (K form)		
Muscovite	2 150 / (6.6)	30 / (6.9)	76 600 /(6.9)
Biotite	9 600 / (7.2)	100 /(7.4)	6 700 / (7.3)
Phlogopite	62 800 / (7.7)	20 / (7.8)	5 700 / (7.8)
	Modified mica minerals (Na form)		
Muscovite	450 / (6.1)	60 / (6.9)	7 200 / (6.7)
Biotite	101 300 / (7.3)	700 / (7.2)	1 400 / (7.2)
Phlogopite	131 400 / (7.8)	950 / (8.2)	8 900 / (8.9)

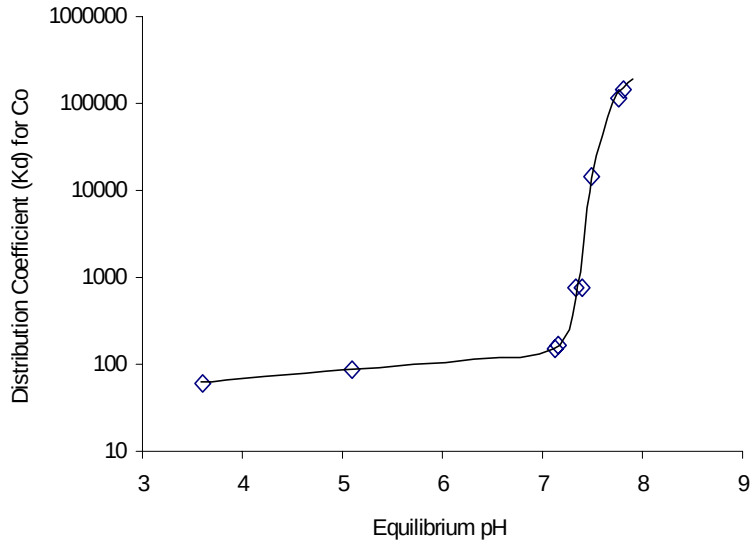

Figure 19. Distribution coefficient of ^{60}Co on sodium-form phlogopite as a function of pH.

4. Summary and conclusions

An extensive series of tin antimonates with from 0 to 100% Sn/Sb substitution were synthesised and the products were divided into three categories according to structure: materials with pyrochlore structure, materials with rutile structure, and materials with a mixture of both. The progressive Sn for Sb substitution of the pyrochlore phase, which is based on the structure of crystalline antimony pentoxide (space group Fd3m), resulted in slight distortion and opening of the tunnel structure. In turn, the Sb for Sn substitution of the rutile phase, which is based on the structure of tin dioxide (space group $P4_2/mnm$), acidified the material and lowered the point of zero charge of the material. These changes in structure had a direct effect on the ion exchange properties of the materials.

The synthesised tin antimonates showed good uptake properties for activated corrosion products, and the Sb/Sn substitution of the materials improved their metal uptake properties in acidic and calcium-bearing solutions. The effects of increasing Sn content on distribution coefficients (K_d) for cobalt and nickel were almost identical for materials with rutile structure and mostly similar for materials with pyrochlore structure. The findings suggest that ordering of the crystals has strong influence on the K_d values of tin antimonates with pyrochlore structure. Cobalt uptake was diminished in the low crystallinity exchangers with distorted pore structure since the majority of the ion exchange sites are located inside the tunnels and cavities of materials with pyrochlore structure. Most of the nickel uptake is proposed to take place at surfaces of the materials, so crystal ordering has less effect on nickel selectivity.

The effect of pH on the distribution coefficients was significant, a typical finding for hydrous metal oxides with their weakly acidic nature. An increase in the K_d values occurred with increasing equilibrium pH and excellent uptake of activated corrosion products was observed from solutions of neutral pH. In particular, rutile-structured tin antimonates showed good uptake of activated corrosion products and tolerance for interfering calcium ions. The metal uptake from acidic solution was also relatively high. Mixed metal oxides with high Sn/Sb substitution in particular exhibited high uptake of activated corrosion products in solutions of low pH. For the fission products, the uptake of strontium was superb on pyrochlore tin antimonate, while the uptake of caesium was

only modest. The uptake of actinides (Pu and Am) was good, but somewhat perplexing and in need of further study.

Granular tin antimonates showed promising column performance for decontamination purposes. Large volumes of solutions, with considerable amounts of competing ions, were decontaminated of nickel and cobalt with high decontamination factors. The kinetics of the ion exchange reaction had a strong influence on the metal uptake and cobalt and nickel selectivity was in reverse order in batch and column experiments. High selectivity of pyrochlore-structured tin antimonates in the batch experiments for cobalt was attributed to ion exchange in tunnels inside the material. The higher breakthrough level of cobalt than of nickel in the column experiment can thus be explained by the restricted flow of ions inside the tunnels of the exchange material, resulting in a lower ion exchange rate for cobalt than of nickel whose uptake occurs mostly on the surface of the exchanger.

On the basis of the good cobalt and nickel uptake both in batch and in dynamic column experiments, the application of tin antimonates for the decontamination of floor drain and neutral bond waters is considered to be a promising possibility. However, further studies on the physical form of tin antimonates are required since clogging of the column beds occurred, particularly in solutions of high calcium concentration. The possible breakage of the material agglomerate structure by further crystallisation of the pyrochlore content needs to be explored.

Data on the uptake of cobalt on tin antimonates can be used in some degree for the prediction of nickel uptake, even though the uptake level of nickel is much lower. The structure and crystallinity of the tin antimonate also needs to be known because of the strong effect of these factors on the metal uptake properties.

The use of mica minerals for the uptake of cobalt is a sound and economical proposition when extreme selectivity is not required. Natural, potassium-form phlogopite exhibited fairly high cobalt uptake, and this was doubled upon its conversion to sodium form. However, the conversion was not easily achieved, so that the gain in metal uptake may not be great enough to justify use of this form.

References

1. K. Dorfner in: K. Dorfner (Ed.), Ion Exchangers, Walter de Gruyter Berlin, New York 1991
2. D.M.C. Horsley and M. Howden, Trans IchemE 68B, 1990, 140.
3. M. Howden and J. Pilot in: D. Naden and M. Streat (Eds), Ion Exch. Technol, Elis Horwood, London, 1984
4. A. Clearfield in: A. Clearfield (Ed.), Inorganic Ion Exchange Materials, CRC Press, Boca Raton, FL, 1982
5. A. Clearfield and J.A. Stynes, *J. Inorg. Nucl. Chem*., 1964, **26**, 117.
6. J. Lehto in: I.D. Wilson (Ed.), Encyclopedia of Separation Science III, The Nuclear Industry: Ion Exchange, Academic Press, 2000
7. G. Kühne in: K. Dorfner (Ed.), Ion Exchanger, Walter de Gruyter Berlin, New York 1991
8. E. Tusa, Proc. Waste Management at Tuscon, Arizona, Feb. 25-March 1, 2001
9. R. Harjula, A. Paajanen, J. Lehto, E. Tusa and P. Standring, Proc. Waste Management at Tuscon, Arizona, Feb. 23-27, 2003
10. D.O. Campbell, Proc. Transactions of the American Nuclear Society, 1989 Winter Meeting. San Francisco, California, November 26-30, 1989
11. J.P. Bibler in: P.A. Williams and M.J. Hudson (Eds.), Recent Developments in Ion Exchange 2, Elsevier, London, UK, 1990
12. B. Miller and P. Tucker, Proc. EPRI LLW Conference, Providence, RI, July 21-23, 1997
13. B.E. Cauthen and J.C. Taylor, Proc. Waste Management at Tuscon, Arizona, Feb. 25-March 1, 1990, 305.
14. O. E. Ekechukwu, L. E. Louckes and R. Hetherington, Proc. Waste Management at Tuscon, Arizona, 1992, 1635.
15. J. Lehto and R. Harjula, *Radiochim. Acta*, 1999, **86**, 65.
16. S.W. Bailey in: S.W. Bailey (Ed.), Reviews in Mineralogy vol 13: Micas,. Mineralogical Society of America, Bookcrafters Inc, Chelsea, Michigan, 1981
17. A. Weiss and E. Sextl, in: Dorfner, K. (Ed), Ion Exchangers, Walter de Gruyter Berlin, New York 1991
18. A.I. Bortun, L.N. Bortun, S.A. Khainakov and A. Clearfield, *Solv. Extr. Ion Exch*, 1998, **16(4)**, 1067.
19. M. Park, D.H. Lee, C.L. Choi, S.S. Kim, K.S. Kim and J. Choi, *Chem. Mater.,* 2002, **14**, 2582.
20. T. Kodama, Y. Harada, M. Ueda, K-I. Shimizu, K. Shuto and S. Komarneni, *Langmuir*, 2001, **17**, 4881.
21. T. Kodama and S. Komarneni, *J. Mater. Chem*., 1999, **9**, 533.
22. T. Kodama, S. Komarneni, W. Hoffbauer and H. Schneider, *J. Mater. Chem*., 2000, **10**, 1649.
23. T. Kodama and S. Komarneni, *J. Mater. Chem.,* 1999, **9**, 2475.
24. A. Deyer in: M. Qureshi and K.G. Varshney (Eds), Inorganic Ion Exchangers in Chemical Analysis, CRC Press, Boca Raton, FL, 1991
25. A. Dyer in: An Introduction to Zeolite Molecular Sieves, John Wiley and Sons, New York, 1988
26. R. Szostak in: R. Szostak (Ed), Molecular Sieves, Van Nostrand Reinhold, New York, 1989

27. J.D. Sherman, *Proc. Natl. Acad. Sci. USA*, 1999, (**96**), 3471.
28. V. Veselý and V. Pekárek, *Talanta*, 1972, **19**, 219
29. A. Ruvarac and A. Clearfield, *J. Serb. Chem. Soc*., 1988, **53(6)**, 283.
30. G. Alberti, *Acc.Chem. Res*., 1978, **11**, 163.
31. P. Olivera-Pastor, P. Maireles-Torres, E. Rodriguez-Castellon, A. Jimenez-Lopez, T. Cassagneau, D.J. Jones and J. Roziere, *Chem. Mater*., 1996, **8**, 1758.
32. A. Dyer, T. Shaheen and M. Zamin, *J. Mater. Chem.,* 1997, **7(9)**, 1895.
33. K.H. Lieser in: Dorfner (Ed.), Ion Exchanger, Walter de Gruyter Berlin, New York 1991
34. A. Clearfield, *Solv. Extr. Ion Exch*., 2000, **18(4)**, 655.
35. D.I. Jacobi and M. Streat, in: L. Cecille, M. Casarci and L. Pietrelli (Eds), New Sep. Chem. Tech. Radioact. Waste Other Specific Appl., Elsevier, London, 1991
36. M. Streat and D.L Jacobi, in: A. K. Sengupta (Ed), Ion Exchange Technology, Technomic Publishing Co., 1995
37. I.M Ismail, M.R. El-Sourougy, N. Abdel Moneim and H.F. Aly, *J. Radioanal. Nucl. Chem*., 1998, **237(1-2)**, 97.
38. E.H. Tusa, A. Paavola, R. Harjula and J. Lehto, *Nuclear Technology*, 1994, **107**, 279.
39. E.H. Tusa, A. Paavola, R. Harjula and J. Lehto, Proc. Radioactive Waste Management and Environmental Remidiation, 8th, Bruges, Belgium, 2001, 1767.
40. L.H. Baestlé, D. Van Deyck and D. Huys*, J. Inorg. Nucl. Chem*., 1965, **27**, 683.
41. J. Lehto, S. Haukka and R. Harjula, *J. Chem. Soc. Dalton Trans*., 1990, 1107.
42. M. Abe in: A. Clearfield (Ed.), Inorganic Ion Exchange Materials, CRC Press, Boca Raton, FL, 1982
43. J.G. Decaillon, Y. Andres, B.M. Mokili, J.C. Abbe, M. Tournoux and J. Patarin, *Solvent Extr. Ion Exch*., 2002, **20(2)**, 223.
44. Y. Xu, J.Q. Xu, G.Y. Yang, G.D. Yang, Y. Xing, Y.H. Lin and H.Q. Jia, *Acta Cryst*., **C54**, 9.
45. R.C Haushalter and L.A. Mundi, *Chem. Mater*.,1992, **4(1)**, 31.
46. J. van R. Smit*, J. Inorg. Nucl. Chem*., 1965, **27**, 227.
47. K.L. Naraqsimharao, K.S. Sarma, C. Mathew, A.V. Jadhav, J.P. Shukla, V. Natarajan, T.K. Seshagiri, S.K. Sali, V.I. Dhiwar, B. Pande and B. Venkataramani, *J. Chem. Soc., Faraday Trans*., 1998, **94(11)**, 1641.
48. R.W.C. Broandbank, S. Dhabnanandana and R.D. Harding, *J. Inorg. Nucl. Chem*., 1961, **23**, 311.
49. C.J. Miller, A.L. Olson and C.K. Johnson, *Sep. Sci. Technol*, 1997, **32(1-4)**, 37.
50. T.A. Todd, N.R. Mann, T.J. Tranter, F. Sebesta, J. Sohn and A. Motl, *J. Radioanal. Nucl. Chem.,* 2002, 254(1), 47.
51. Y. Onodera, H. Mimura, T. Iwasaki, H. Hayashi, T. Ebina and M. Chatterjee, *Sep. Sci. Technol.,* 1999, **34(12)**, 2347.
52. J. van R. Smit in: M. Qureshi and K.G. Varshney (Eds), Inorganic Ion exchangers in Chemical Analysis, CRC Press, Boca Raton, FL, 1991
53. S. Solbrå, N. Allison, S. Waite, S.V. Mikhalovsky, A.I. Bortun, L.N. Bortun and A. Clearfield, *Environ. Sci, Technol*., 2001, **35**, 626.

54. D.M. Poojary, R.A. Cahill and A. Clearfield, *Chem. Mater*., 1994, **6**, 2364.
55. D.M. Poojary, A.I. Bortun, L.N. Bortun and A. Clearfield, *Inorg. Chem*., 1996, **35**, 6131.
56. J.F. Walker, Jr., P.A. Taylor and D.D. Lee, *Sep. Sci. Technol*., 1999, 34(6&7), 1167.
57. A. Clearfield, *Solid State Sciences*, 2001, **3**, 103.
58. E.A. Behrens, D.M. Poojary and A. Clearfied, *Chem. Mater*., 1996, **8**, 1236.
59. A. Dyer, M. Pillingern and S. Amin, *J. Mater. Chem.,* 1999, **9**, 2481.
60. T. Möller, Doctoral Dissertation, 2002, ISBN 952-10-0412-6, University of Helsinki
61. T. Möller, A. Clearfield and R. Harjula, *Micropor. Mesopor. Mater.,* 2002, **54(1-2)**, 187.
62. T. Möller, R. Harjula, M. Pillinger, A. Dyer, J. Newton, E. Tusa, S. Amin, M. Webb and A. Araya, *J. Mater. Chem*., 2001, **11(5)**, 1526.
63. http://www.nrc.gov/reading-rm/doc-collections/nuregs/staff/sr1437/v1/fig021.gif
64. M. Abe and K. Sudoh, *J. inorg. nucl. Chem.,* 1980, **42**, 1051.
65. M. Abe and T. Itoh, *J. inorg. nucl. Chem.,* 1980, **42**, 1641.
66. L.H. Baetsle and D. Huys *J. inorg. nucl. Chem.,* 1968, **30**, 639.
67. R. Rãutiu and D.A. White, *Solv. Extr. Ion Exch.,* 1996, **14(4)**, 721.
68. M. Abe, Bull. *Chem. Soc. Jpn*, 1979, **52(5)**, 1386.
69. J.D. Donaldson and M.J. Fuller, *J. inorg. Nucl. Chem.,* 1968, **30**, 1083
70. M. Qureshi, V. Kumar and N. Zehra, *J. Chromatogr.,* 1972, **67**, 351.
71. M. Abe and N. Furuki, *Solv. Extr. Ion Exch.,* 1986, **4(3)**, 547.
72. M. Tsuji, H. Kaneko, M. Abe, Y. Morita and M. Kubota, *Radiochimica Acta*, 1993, **60**, 93.
73. M.M. Abdel-Badei, I.M. El-Naggar, A.A. El-Belihi, H.M. Aly and H.F. Aly, *Radiochimica Acta*, 1992, **56**, 89.
74. N. Burham, S.H. Abdel-Halim, I.M. El-Naggar and M.F. El-Shahat, *J. Radioanal. Nucl. Chem*., 1995, **189**, 89.
75. I.M. El-Naggar, E.I. Shabana and M.I. El-Dessouky, *Talanta*, 1992, **39**, 653.
76. R. Rãutiu and D.A. White, *Solv. Extr. Ion Exch.,* 1996, **14(4)**, 721.
77. D.A. White and R. Rãutiu, *Chem. Eng. J.,* 1997, **66**, 85.
78. J. Chang, Table of Nuclides, KAERI, http://atom.kaeri.re.kr/ton
79. P. Karhu, T. Möller, R. Harjula and J. Lehto, Ion Exchange at the Millennium, Proceedings of IEX 2000, 8th, Cambridge, United Kingdom, July 16-21, 2000
80. J. Lehto, L. Brodkin and R. Harjula, *Nucl. Technol.* 1999, **127**, 81.
81. C. Pepelis, K.F. Hayes, and J.O. Leckie, HYDRAQL: A Program for the Computation of Chemical Equilibrium Composition of Aqueous Batch System Including Surface-Complexation Modeling of Ion Adsorption at the Oxide/Solution Interface, Technical Report No.306, Dept. of Civil Engineering, Stanford University, Stanford, Ca, 1988
82. R.D. Shannon, *Acta Cryst*., 1976, **A32**, 751.
83. T. Nütz and M. Haase, *J. Phys. Chem. B* , 2000, **104**, 8430.
84. J. Rockenberger, U. zum Felde, M. Tischer, L. Tröger, M. Haase and H. Weller, *J. Chem. Phys.,* 2000, **112**, 4296.
85. T. Nütz, U. zum Felde and M. Haase, *J. Chem. Phys.,* 1999, **110(24)**, 12142.

86. S. Shanthi, C. Subramanian and P. Ramasamy, *J. Cryst. Growth*, 1999, **197**, 858.
87. K.C. Mishra, K.H. Johnson and P.C. Schmidt, *Phys. Rev. B*, 1995, **51(20)**,13972.
88. J.P. Coleman, A.T. Lynch, P. Madhukar and J.H. Wagenknecht, *Sol. Energy Mater. Sol. Cells*, 1999, **56**, 375
89. S. B. Hendrick and M. E. Jefferson, *Am. Mineral*., 1939, **24**, 729.
90. A. D. Scott and M. G. Reed, *Soil Sci. Soc. Proc.,* 1962, 41.
91. T. Möller, A. Clearfield and R. Harjula, *Chem. Mater*., 2001, **13**, 4767.
92. D.A. White and R. Rautiu, Chem. *Eng. Journal*, 1997, **66**, 85.
93. Y.J. Marcus, *Chem. Soc., Faraday Trans*., 1987, **83**, 2995.
94. M. Abe, and N. Furuki, *Bull. Chem. Soc. Jpn*., 1985, **58**, 1812.
95. H.F. Aly and I.M. El-Naggar, *J. Radioanal. Nucl. Chem.,* 1998, **228**, 151.
96. H. Lahr and W. Knoch, *Radiochimica Acta*, 1970, **13(1)**, 1.
97. G. Choppin, J. Rydberg and J.O. Linjenzin in Radiochemistry and Nuclear Chemistry, Butterworth-Heinemann Ltd, Oxford, 1995, 414.